IGEN 430: Final Report

Group 11: Halo: Anti-Whiplash Car Head Restraint

Arjav Prasad, Lucas Petersen, Sena Akalp, Charlie Lever, Ishaan Sareen, Kayla Butcher

Executive Summary

Halo is an innovative whiplash prevention system, engineered to track head movement of a vehicle occupant and upon rear impact move into a predetermined safe distance from the user's head, effectively preventing neck rotation and associated injuries such as hyperflexion and hyperextension – also known as whiplash trauma. Conventional headrests consist of a mounted static foam block on a manually adjustable height mechanism, preventing whiplash when the head of the passenger is properly aligned. Unfortunately, achieving correct alignment is infrequent as head position changes throughout travel, and often headrests are not adjusted when getting into the vehicle. Whiplash trauma is a debilitating injury as it can stay with victims throughout their lifetime – even when the majority of rear end collisions occur below 12 miles per hour.

Halo aims to reduce whiplash and the lack of occupant adjustment of head restraints by creating an active monitoring system with auto-positioning of the headrest and passive damping upon impact to reduce the incidents of whiplash in low-speed, rear impacts. Incorporating LiDAR sensors for precise position tracking, motor-driven telescoping actuation for horizontal movement, rack and pinion actuation for the vertical actuation, and a proprietary control loop, our system represents a groundbreaking approach to enhancing vehicle safety.

The system functions through the integration of the mechanical, electrical, and software subsystems – sensing the crash, gathering the sensor distance, then actuating the mechanical system. The sensors that are installed in the headrest will track the positions of the driver's head in real time, sending positional information to our on-board microcontroller. The controller then interprets this data and actuates the headrest into an optimal position through a telescoping actuator. Once impact is imminent, our system features holding torques for the horizontal and vertical systems to remain in place, and the user's head is cushioned through shock absorbers.

A major design constraint for this project was to make the system sleek so that it does not impede the passenger behind the occupant. To achieve this, a telescoping actuator was used to allow for 143% extension and no impact to the rear passenger, the occupants head restraint remained in its optimal position through the mounting plate which translated the mounting pins rearward from the vehicles original positioning and is easily swappable to accommodate a variety of automaker's vehicles.

As part of our 430 constraint, we had a maximum allowable budget of $1000 that went into the prototyping and production of this project. The majority of our budget was spent on materials such as aluminum stock, electrical components made up of the microcontroller, stepper motors, and sensors, and the assembly components such as the linear rails, specialty length fasteners, and rack and pinion.

A sustainable disposal is being implemented to recycle and repurpose as many parts as possible. All of the printed materials used for prototyping are recycled through the IGEN 3d Print shop, and the aluminum stock returned to the IGEN mechanical shop for future reuse. The electrical components were distributed among the members of our group and the final assembly parts for the mechanical system were taken home by the mechanical team for future personal projects.

Problem Definition

Objectives

The current prevalence of whiplash injuries in vehicle accidents, underscored by the lack of innovation in the field of headrest design, highlights the space available in the industry for an advanced head restraint solution. Our team has a crucial objective of engineering a system capable of automatic alignment with the occupant's head, ultimately reducing whiplash trauma in vehicle occupants. This area of automotive innovation is of great interest to not only users but vehicle manufacturers to improve their product perception and the insurance industry which puts millions of dollars worth of resources into claims and research for whiplash injuries each year.

Traditional static foam block headrests, manually adjustable in height, lack positional adaptability during travel as achieving proper alignment is challenging with a dynamic head position. This issue is further compounded as the headrest position is often overlooked when entering the vehicle, leaving room for injuries in the event of a rear-impact crash. Our primary users, encompassing both vehicle drivers and passengers, stand to benefit significantly from this advancement.

Users, Needs & Constraints

The primary users of this product are vehicle occupants, focusing on the driver and passenger. These users are in direct contact with our product. Secondary users of this system are the vehicle manufacturer's and auto insurance companies and policy makers.

The needs of our users, the vehicle occupants, are threefold: safety, usability, and integration into existing systems. The product needs to ensure safety by reducing whiplash injuries through a redundant safety system, usability by adapting to users cars easily by adapting to different car models and without loud noises or discomfort, and integrate into a standard 24V system.

Amidst these needs, our project encounters certain constraints that demand careful consideration. Challenges included designing a compact, efficient system within the limited space of a vehicle and maintaining performance in terms of speed, safety, and damping. Our approach utilized the standard headrest pin connections for easy installation across a multitude of vehicles. Managing cost was a financial constraint, which required balancing the performance of the components with economic viability given the limited budget through the integrated engineering program. In order to keep under budget, our team utilized the 3D Print Shop in the IGEN work space as well as resources in house such as the stock plate and the CNC machines where we machined our own parts.

Whiplash injuries often occur at low-speed rear impact due to the abrupt deceleration experienced by the occupants of the vehicle. In an impact, the neck of the occupant rapidly travels back, flexural deformation of the neck is observed, then the cervical spine assumes an S-shaped curve as lower vertebrae first extend followed by upper vertebrae, and finally the entire neck is extended to extension moments at both ends of

the spine. In this process, the spinal cord is pinched or damaged leading to issues such as chronic neck pain, breathing, head movement, and other vital functions.

Whiplash can be prevented by correctly positioning the head restraint to be level with the top of the head, and sit less than three inches away from the back of the head. To address this problem, our team has designed a comprehensive solution that integrates positional monitoring, x- and y-translation of the system, and passive damping. The is a sleek, quiet, and effective system which reduces whiplash injuries by correctly positioning itself with the occupant's head.

Design Requirements

Table 1: Design requirements

Requirement Category	Specific Requirement	Justification	Quantitative Range/Limit
Safety	Reduction of whiplash injuries	To protect occupants in rear-impact crashes	Whiplash injury reduction by 75%[1]
	Redundant safety system	To ensure reliability and prevent system-induced risks	Two-fold safety mechanism
Usability	Automatic head alignment	To adapt to dynamic positions of the occupant's head	Response time within 1 second[2]
	Quiet operation	To maintain a comfortable and non-distracting driving environment	Noise level below 40dB[3]
	Non-interference with driving/comfort	To ensure the system doesn't disrupt the driving experience	Ergonomic design parameters
Integration	Compatibility with 24V vehicle system	To facilitate easy integration into existing vehicles	24V power requirement
	Retrofit capability	To allow easy use across different vehicle models	Compatible with sedans, SUVs and hatchbacks
Space and Mounting Constraints	Compact design	Due to limited space within vehicles	Dimensions within 30 cm by 40 cm by 15 cm[4]
	Standard headrest connections	For compatibility with existing seat structures	Compatible with 80% of vehicles

---

[1] Previous headrests designed to prevent whiplash have potential to reduce such injury by 75% https://www.newscientist.com/article/dn2153-pop-up-headrests-cut-whiplash-injuries/#:~:text=Headrests%20design ed%20to%20prevent%20whiplash,to%20the%20first%20field%20study
[2] Windsor Machine Group promises timing of less than one second
[3] Typical vehicle interior noise levels range from 40 to 70 decibels https://www.driverknowledgetests.com/resources/choosing-a-quiet-car-and-how-cabin-noise-affects-your-concentrat ion/
[4] Based on FMVSS NO. 202

	No negative impact on rear passengers	To ensure safety and comfort for all occupants	Safety clearance standards
Cost Management	Cost-effective design	To adhere to allotted budget	Budget limit of $1000
Time Constraint	Efficient design process	To adhere to project timeline	Completion before April 10, 2024

Introduction

Within automotive safety, innovation is often driven by vehicle safety standards and changing technological advances. To further advance these standards, our team has tackled the redesign of the vehicle head restraint. This innovative response to a critical gap in the current safety features, specifically addresses whiplash injuries which occur during rear-end vehicle impact collisions.

Whiplash is the hyper-extension and hyperflexion of the neck, causing injury to the spinal cord which can last with passengers for a lifetime of chronic pain. Despite the prevalence of whiplash injuries, particularly in low speed impacts, conventional safety mechanisms are static and often overlooked and unadjusted by vehicle occupants [1]. Recognizing this, our team has designed a system capable of continuously monitoring head position and auto-positions the headrest to ensure the headrest is in a safe range upon impact of the vehicle. The system also features a passive damping mechanism, which reduces impact forces seen by the head and lowers risk of injury. The Halo project combines precision sensing, custom mechanical design, and an understanding of injury biomechanics to create an active monitoring and positioning system for car headrests.

The team reviewed technical studies on car headrest design, notably one by AEDS's Special Interest Group [2]. This research, which detailed the use of hydraulic and pneumatic systems to adjust headrests, inspired our initial design considerations. However, due to budget constraints, we decided against these systems. The AEDS study provided CAD models of the headrest's internal assembly, which were crucial for understanding construction details. Our goal is to develop a sleek, quiet system that effectively positions the headrest to minimize whiplash injuries.
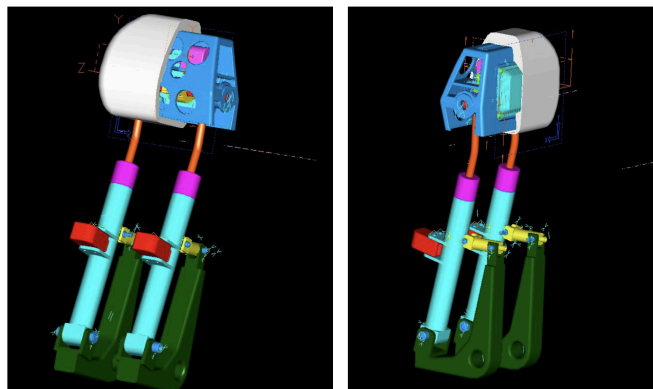

Figure 1: Interior CAD Assembly Design of Car Headrest created by AEDS team

Safety

Our team is committed to safety throughout the entire design process. We ensure that we follow the metal and electrical shop rules as to not endanger ourselves or others while we build. We wear safety glasses when working with electrical wiring or with metal tools. We use hearing protection when working with loud machining tools and we encourage others in the shop to do the same while we are working. The largest source of safety risk comes from the mechanical system of our component. Parts of our hands could get caught in the mechanical frame if we are not careful. We do a final safety check to ensure there is no possibility of anyone getting hurt when the power is turned on and the motors begin to move. We are using a relatively low voltage and current for our project. Regardless, we follow a similar procedure of doing a final check before turning on the voltage supply and having power run through our boards and wires.

Methods and Design

Engineering Calculations

Force on Impact

During a rear-end collision, the force exerted on the head or neck as it impacts the headrest can determine the potential for whiplash injuries. Our analysis, derived from a combination of real-world data and laboratory tests, suggests that the head can be subject to forces ranging between 500 to 1000 N. The impact of this force onto the components such as the actuator and pins can be seen in Appendix F.

Force Estimation

Utilizing data from the NHTSA study and factoring in head accelerations ranging from 3.3g to 7g, combined with an average head mass of 4.75 kg, we derived a comprehensive force estimation model. This model delineates the various forces the proactive headrest system will need to counteract to prevent injuries

$$Lower\ limit: 3.3\ X\ 4.75\ X\ 9.81 \approx 153.5\ N$$
$$Upper\ limit: 7\ X\ 4.75\ X\ 9.81 \approx 328.7\ N$$

Acceleration Estimation

Using the data from the NHTSA, we have found that the head acceleration is at least two and a half times larger compared to the peak vehicle acceleration. While average vehicle acceleration in a small rear end collision was found to be approximately between 3 and 5 m/s2, the average head acceleration was calculated to be between 7 to 13 m/s2 approximately. Which is a significant difference and hence creates a big safety factor.

$$Ah\ =\ 2.75Av\ -\ 0.89$$

Where: Ah = Head acceleration

Av= Vehicle acceleration

Correlation index R2 = 0.80

Sample Calculations

Table 3: Sample Calculations of vehicle and head acceleration

Average vehicle acceleration (m/s2)	Average head acceleration (m/s2)
3.0	7.36
4.0	10.11
5.0	12.86

Experimental Methods - Sensor Design

Accelerometer - MPU 6050

The MPU 6050 accelerometer is integral to our impact detection design, chosen for its precision in multi-axis acceleration measurement. In rear-end collisions, accurately detecting the vehicle's rapid deceleration is crucial. The MPU 6050's ±16g range allows for monitoring extreme ranges of acceleration, from minor jolts to severe impacts.
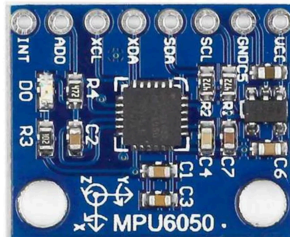
Figure X: MPU - 6050 module

This accelerometer distinguishes itself with a 1 kHz sampling rate, ensuring high-resolution data capture, which is vital for the timely activation of safety mechanisms. Utilizing an I2C protocol, it offers a streamlined and efficient communication pathway, which is particularly advantageous in a system where latency can compromise safety outcomes.

VL6180 - Time of Flight Distance Sensor

The VL6180 time of flight distance sensor has a narrow field of view which allows it to sense the points directly on the head rather than sensing the surroundings. This makes it an optimal choice for the headrest due to its performance and precision in distance measurements in confined spaces. In the head movement test, the VL6180 time of flight distance sensor performed significantly better compared to other distance sensor alternatives such as the HC-SR04 ultrasonic sensor, which was previously considered for this project but got replaced with the time of flight sensor. The sensor proved to be reliable and suitable for

use in the headrest where precision is a crucial element. The VL6180 vs. HC-SR04 sensor test results are seen in Appendix A.

The sensors are utilized for three points on the head using three sensors. The distance sensors will detect the distance of the head from the headrest in three different points and move the headrest according to the feedback of these distances. A preliminary flowchart of this movement was made to understand the required actions based on these distance measurements. The logic was then coded in Arduino in order to further test the sensor system, as seen in Appendix B.

ESP32 Microcontroller

The ESP32 has been selected as the core processing unit for its exceptional computational speed and compact size, crucial factors in our design for an efficient and space-conserving impact detection system. Its processing capabilities, around 60 times faster than the Arduino, significantly reduce system response time, a key parameter in our design goals.

With onboard WiFi and Bluetooth, the ESP32 supports real-time data transmission, enabling our system to communicate instantly with external devices and networks for diagnostics and system updates. The multi-protocol capability, including I2C, SPI, UART, and CAN, provides comprehensive interfacing options, allowing our design to be modular and flexible, ready to integrate a wide range of sensors and components.

Experimental Methods - Mechanical Design

Y-Movement

Our Y-movement design evolved through several iterations. Initially, we planned to attach a motor to the car seat's metal frame, using modified notched pins (typical in standard headrests for manual adjustment) as a linear gear to precisely move the headrest up and down. However, this setup lacked convenience. We simplified by integrating the motor directly into the headrest, hidden under the damper for a cleaner look and eliminating the need for external setup. Originally, the design used a stepper motor connected to two gears and dual rack and pinion systems for bilateral support. Due to complications in frame design and gear sizing, we streamlined this to a single rack and pinion, achieving sufficient precision and reliability with less complexity.
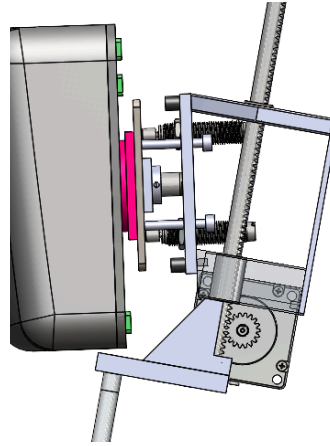
Figure: Rack and Pinion System

We refined our design by separating the mounting and actuation pins, simplifying the frame and enhancing maintainability. This adjustment eliminated the need for complex part shapes and allowed for straightforward assembly and maintenance access. The motor was strategically placed under the chassis to avoid interfering with other components and to keep gear mechanisms clear of sensor wiring.

This streamlined setup preserved the headrest's vertical adjustability while improving manufacturability and assembly ease. We used stepper motors capable of handling the headrest's weight (predicted to be under 2000 grams) and powered them through the 12V socket already used for the headrest, with power cables neatly organized in a cable chain along the seat's side.

The stepper motor must be able to resist the torque applied by the weight of the headrest. The total torque will be the calculated using the following:

*Weight of headrest = Mass of headrest * 9.8m/s^2*

*Torque applied to the stepper = Weight of the headrest * Radius of the stepper motor gear*

Using the above formula we see that the torque experienced by the stepper motor is going to be proportional to the mass of the headrest so by making the headrest light weight we can effectively choose our stepper motor that can support that kind of torque. Our expected weight of the headrest system was 2000g so we specified a motor with a 1.28 Nm holding torque which could accommodate a maximum weight of 5kg using our pinion gear radius as our reference.

X-Movement

For the x-movement of our system a telescoping actuator is used incorporating helix-style threads for rapid movement often seen in 3D printing machines and gantry system lead screws. The telescoping actuator extends and retracts with rotational motion to achieve linear actuation through a two-stage actuation method. The elements of the actuator extend sequentially, allowing for 143% extension.

The actuator consists of five layers: the lead screw, secondary screw, and three linear sliding components as can be seen in the figures below. (Split Views In Appendix G)
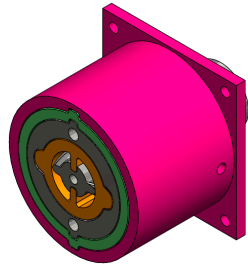
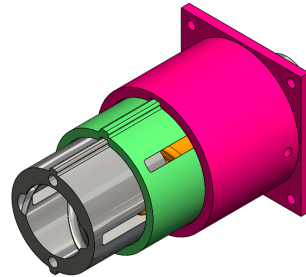Figure: Isometric View (Compressed) Figure: Isometric View (Extended)

The method of actuation for this component is the following steps:
The motor drives the central gray lead screw to actuate the system. This screw threads through the green second linear sleeve, pushing it forward. The secondary orange screw, coupled to this sleeve via a bearing filled with 3mm steel balls, rotates through interaction with the lead screw's 'wings' sliding in its channels. This rotation extends the secondary screw, which drives the internal thread of the first gray linear sleeve, fully extending the actuator.

To ensure the extension mechanism performed effectively, the correct stepper motor was chosen to overcome both the thread friction and the additional weight of the foam headrest, while also providing enough holding torque (25.03 N-mm) to prevent retraction upon impact. A NEMA 17 motor with a 5:1 planetary gearbox was selected, offering a 30 N-mm output torque – comparable to a NEMA 23 but with a more compact and lightweight design. This motor is compatible with the TB6600 Stepper Motor Driver for independent operation. All the calculations for stress, impact, and motor sizing can be seen in Appendix F.

Damping system:
In our headrest, a pivotal subsystem is the damping system as it reduces the amount of force experienced by the head in the event of a collision. Our system is made up of 2 damper-spring shock absorbers that lie between the interstitial plate assembly and the actuator plate of our headrest.
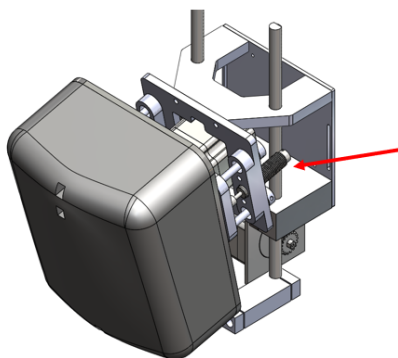
Figure X: CAD of Damper Location Figure X: Prototype with Dampers Integrated
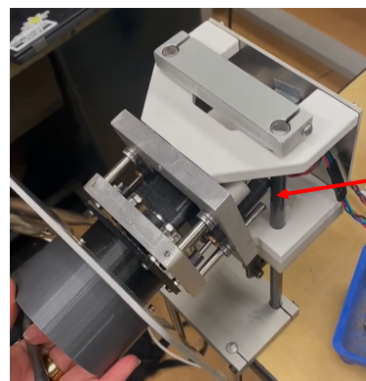
For the dampers, it was determined that the needed energy absorption was 77.875 Nm to sufficiently offset the impact and reduce ricocheting of the head. In order to achieve the level of energy absorption

8

needed, off the shelf industrial grade shock absorbers were used from McMaster and integrated into the system by threading into the interstitial plate. Calculations for the sizing of the damper components can be seen in Appendix F.

Material Selection

Foam Head Block

The foam block, acting as the primary contact point of the head restraint, functions similarly to traditional headrests by absorbing impact and offering comfort and ergonomic support. Made of polyurethane for its ideal density and durability, it effectively dissipates energy during collisions to reduce whiplash risks. The selection of the appropriate polyurethane type was determined through simulations and calculations of foam deflection and energy absorption, detailed in Appendix F.

Actuator

The material used for the telescoping actuator is Durable resin from Form Labs. This resin was selected for the impact strength and resilience of the material. The main criterion for material selection was manufacturability and impact strength. As the component will be load bearing in the event of a crash, the resin was selected for its high impact strength. Further calculations can be seen in Appendix F and simulations in Appendix G.

Final Design Evaluation

Detect Crash

The final crash detection system combines LiDAR and accelerometer sensors to improve safety. The VL6180 LiDAR sensor, mounted at the rear of the vehicle, detects potential rear-end collisions by monitoring the distance to the following car. The MPU 6050 accelerometer serves as a redundancy, detecting impacts directly to ensure the system functions under various lighting conditions where LiDAR may fail. Although the accelerometer reacts as the crash happens, potentially losing crucial response time, it still significantly mitigates neck injuries by rapidly positioning the head restraint. The system uses both sensors to quickly adjust the head restraint accurately at the moment of detection, minimizing the injury risk during rear-end collisions.

Sense Head

The final head sensing design utilizes three VL6180 laser time of flight distance sensors to measure the distance from the headrest to the head at three points, as mentioned in the Experimental Methods section. This configuration ensures accurate tracking of the head in both the x- and y-direction, and allows the system to reposition the head restraint according to these measurements. The VL6180 sensors use I2C communication, and they all connect to the same I2C channel on the ESP32. These sensors are unable to permanently change their default I2C address, which is 0x29. This requires new independent addresses to be configured to each sensor upon startup using the XSHUT pins. For the brain assembly, the sensors and accelerometer are wired to the ESP32 using the same I2C channel, three different pins to control the shutoff, and a common 5V power and ground pin. The wiring diagram is in Appendix C, along with the

configuration of the three sensor system, to illustrate the placement of each sensor. Further iterations were made in the head sensing system, including altering the code to determine the exact movements (x- and y-direction, in millimeters) that need to be made by the head restraint, as opposed to simply indicating what direction to move in. The sensor code was also incorporated with the crash detecting system, in order to only move the head restraint when a crash is detected.

Move Head Restraint

This design uses a telescoping actuator powered by a DC motor for horizontal adjustments of the headrest, allowing it to move forward or backward. Vertical movements are managed through a rack and pinion mechanism, where steel pins, acting as the rack, pair with a gear (the pinion) to smoothly raise or lower the headrest. These mechanisms provide multi-directional adjustability, ensuring precise, ergonomic positioning for enhanced comfort and safety. System drawings are in Appendix F.

Testing and Validation

Testing

Crash Test Procedure

The objective of the crash test procedure was to assess the effectiveness of the Halo head restraint system under simulated rear-end collision scenarios. We aimed to validate the system's ability to prevent whiplash injuries by accurately positioning the headrest relative to the occupant's head during an impact.

The sled, equipped with the car seat and Halo head restraint system, was accelerated to speeds that replicate common low-speed rear-end collisions. We used the Neck Injury Criterion (NIC) as our benchmark to evaluate the risk of injury.

The Procedure:

1. Impact Simulation
   - Rear impact tests conducted at various speeds.
   - Repeated test with different headrest positions.

2. Data Recording
   - Data recorded during impact.
   - Sensors used to record data:
     - Impact force from the head
     - Compressive force on the neck

3. Post test
   - Analyze recorded data and compare against some injury criteria. (See NIC: Neck Injury Criterion)
   - Compare the performance of the headrest.

Test Dummy Specifications

A test dummy, designed to mimic the weight distribution and kinematics of the human body was used. The head of the dummy was weighted to represent an average human head, and the neck assembly was articulated to allow for accurate simulation of cervical spine movement during a collision. The head (Volume = 3.5 liters) was filled with aquarium gravel with a density of 1.5 g/cm3 to give it a final mass of around ~ 4.3 kg to accurately reflect the weight of the human head.

Requirements for a Suitable Articulated Neck:

- Be able to realistically simulate head impact events.
- Consist of at least three cervical vertebrae if the neck motion ranges are fully achieved.
- The neck motions are considered in terms of flexion angles from 50° and extension up to 80°; rotation angles 140° (70° to each side) and lateral bending 45° to each side for the complete neck motion range.
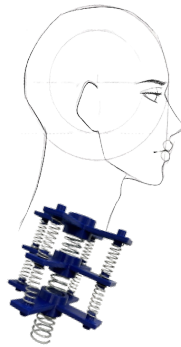
Figure X: Redesigned Articulated Neck

Figure X: Assembled Testing System

Sled Test

The crash test was conducted using a dynamic sled system designed (see above) to emulate a vehicle's movement during a rear-end collision. The sled is composed of rails that guide the sled's trajectory and a platform where the car seat and head restraint system are mounted. The rails ensure a linear trajectory for repeatability, reducing variability between tests. The sled is required to support the weight of both the test dummy and the car seat, without altering testing performance. It is also required to accelerate 3 - 5 m/s^2 to mimic rear end collision and reach the required velocities of 5 - 10 mph for a suitable whiplash test. These requirements ensure proper data tracking is available and relevant to rear end collisions and whiplash injuries. The sled must decelerate slowly to mitigate excess strain on the test dummy and limit external variables. Stoppers were used at the ends of each rail to lengthen deceleration time.

Initial Positioning: The dummy was positioned in the car seat with its head in a neutral position, as a typical occupant would be.

Impact Simulation: The sled was then propelled along the rails at controlled speeds, simulating the forces of a rear-end collision.

Data Collection: Sensors attached to the dummy and the headrest system collected data on the acceleration forces experienced by both the head and neck, as well as the headrest's movement and positioning in response to the simulated collision.

Safety Measures: Throughout the test, the system's safety features were evaluated to ensure no additional risks were presented to the dummy, replicating a real occupant's experience.

Tracking System

The prototype incorporates two distinct force-sensing resistors (FSRs) - one square and one narrow - to measure the force exerted on the headrest and seat, respectively. These sensors provide critical data to evaluate the system's response during simulated impact events. To capture the kinematic response of the head and torso, we employed two accelerometers. The ADXL345 accelerometer, known for its precision, was chosen to monitor torso movements, while the MPU-6050, which can measure both acceleration and angular rotation, was selected for head movement tracking. The relative motion of the torso and head is important when considering the likelihood of neck injury hence the need for two accelerometers. Both accelerometers are interfaced via the I2C protocol which allows for fewer connections to the microcontroller.

The system is interfaced with an ESP-32 microcontroller, selected for its Wi-Fi capabilities, allowing for real-time data transmission to our cloud dashboard. The dashboard displays real-time sensor data, offering immediate insight into the performance and reliability of the headrest during testing scenarios.

MPU 6050

The MPU-6050 sensor is at the heart of our head movement tracking system, combining a 3-axis gyroscope and a 3-axis accelerometer to provide motion analytics. It captures details of head acceleration and angular velocity, essential for understanding the dynamic response of rear impact scenarios. The measurement of these two quantities allows for analysis of not just linear forces but also rotational movements that are critical in the assessment of potential neck injuries.

As shown in the image below, rear collision events cause sudden movements in the neck and head. While acceleration data is useful to describe the resting and impact stages, angular rotation is useful in describing the hyperextension and hyperflexion stages of rear impact collisions.

ADXL 345
The ADXL345 accelerometer monitors the torso's kinematic response. Known for its precision and low power draw, it plays a role in measuring the torso's accelerations, thereby enabling a complete understanding of the body's reaction during rear impacts. The information from the ADXL345 is vital for cross-referencing head movement data, offering a more comprehensive picture of the forces at play during collision events.
FSR

The square force-sensing resistor is integrated into the setup to directly detect and measure the intensity of impacts to the head. Responsive to variations in force, it is calibrated and programmed to activate the data recording sequence upon detecting a level of pressure (force). This ensures immediate logging of critical data following an impact, which is vital for real-time analysis. Its contributions are crucial in timing the accelerometer data, allowing for an approach to understand the forces involved.

Overview
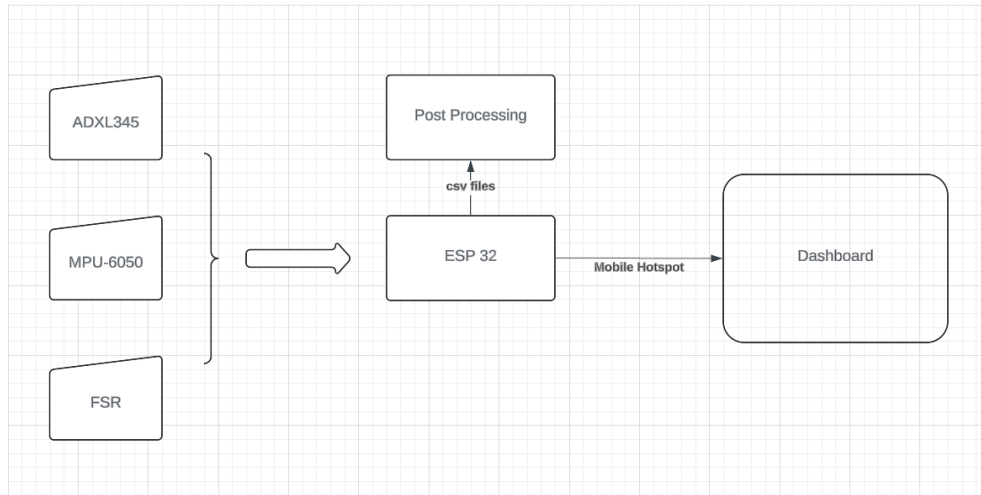
Two separate scripts were running in unison on the ESP-32. The main code i.e, the sensor reading code that interfaces with the different sensors and uses logic statements to ensure timely sensing of head and torso movement. The main code invokes "thingProperties.h" (shown in Appendix E). The "thingProperties.h" script is the unique segment of code that allows for connection between the ESP 32 and the dashboard (via the mobile hotspot connection). After the microcontroller has successfully connected to the cloud, the sensor variables are relayed to the dashboard at a desired rate.

The completed dashboard is shown in Appendix E. The top two graphs show force sensor responses. The next two graphs (2nd row) show the different accelerometer responses, note that the a2 graph (right) is for the head-neck assembly and captures the oscillatory movement whereas the accel graph (left) is for the torso that has minimal oscillatory movement (strapped to the seat). The third and final row show singled out values of head and torso accelerations.

Validation

Data from the tracking system was used to validate the functionality of the head restraint system.

Primary Validation Sequence

    1. Head Impact Detection

To assess the reliability and accuracy of our head impact detection system, we conducted a series of controlled impact tests. The results indicate the system's adeptness in registering an impact. The sharp spike in the graph represents the instant at which the force was applied to the sensor, demonstrating a clear and detectable response from the system. This immediate and distinct detection is crucial for ensuring the system's effectiveness in real-world applications where timely alerts are paramount.

2. Measurement of Force Response (decay analysis) and impulse

In addition to measuring the force response, our system calculates the impulse delivered during an impact. Impulse, the product of force and the time interval over which it acts, provides a comprehensive picture of the impact's severity. Figure Y illustrates the force response over time, allowing us to not only analyze the decay profile post-impact but also to calculate the total impulse.

By integrating the area under the curve in the force vs. time graph, we obtain the impulse imparted to the sensor. This calculation estimates the momentum change that an object undergoes during an impact, which is a critical metric for injury biomechanics. The ability of our system to measure both peak force and impulse is essential in assessing our main systems effectiveness and understanding the nuances of impact absorption. The foam material selection and telescoping actuator design were based on many factors of which impulse was one of them. The x actuation aims to increase the impact duration to reduce neck injury. The use of polyurethane foam was verified as a good choice owing to its ability to dissipate energy.

3. Time calculation algorithm

The algorithm for calculating the time intervals between sequential peaks and their subsequent return to baseline (denoted as Δt) is a critical component for understanding the system's reaction speed. As indicated, the system's decay times ranged from 0.7 to 1.3 seconds. This swift reaction capability is significant for any safety-critical system, where delays can be the difference between prevention and injury.

The **Neck Injury Criteria** is a common metric used to assess the severity of neck injury:

$$N_{IJ} = \frac{F}{Fzc} + \frac{My}{Myc}$$

Where F is force at the head-neck transition point and My is the total moment. The Fzc and Myc values are critical values that can be considered transition points (Fzc,Myc) for sufficient injury. The critical values are specific to the test system - depending on the test dummy build. The Neck Injury Criteria is an agreed upon criteria commonly used by the NHTSA (National Highway Traffic Safety Administration) in safety testing. However, given the resources and time constraints of this project the use of this criteria is not feasible.

To improve the responsiveness of the actuation and head position tracking, future iterations of this project could include the use of head acceleration vs vehicle acceleration data (see previous section). The use of this data and forecasting techniques could improve the detection of rear ended collisions and hence the overall system.

Project Planning

Plan vs. Delivery Table

Task	Start Date	Delivered Date	Notes
3D Print Actuator + Spec Motor	8-Jan-24	24-Jan-24	Redesign Happened over break -- many reprints needed for actuator tolerances
Integrate Motor + Sensors	15-Jan-24	28-Jan-24	Motors hooked up to the sensors
Test Rig Designed	22-Jan-24	30-Jan-24	Test rig in process
Full Prototype V2	29-Jan-24	22-Feb-24	3D Printed Parts received
Test Rig Manufacturing	5-Feb-24	15-Mar-24	The testing setup was designed.
Full System Test 1	12-Feb-24	1-Mar-24	The NEMA 17 without gearbox too weak for headrest
Reading Break	19-Feb-24	8-Mar-24	
System Iteration	26-Feb-24	29-Mar-24	Integration with Electrical system
Redesign	4-Mar-24	22-Mar-24	Parts request to the Materials Shop
Redesign Implementation	11-Mar-24	29-Mar-24	Receive parts
Testing + Validation	18-Mar-24	5-Apr-24	Using the parts from Machine shop, new prototype put together
Full System Test 2	25-Mar-24	6-Apr-24	Full system test occurred, needed to replace NEMA 17 and remake plates for NEMA 23
Testing + Validation + Report	1-Apr-24	7-Apr-24	Testing and Validation occurred the three evenings before DAID.
DAID on 11th	8-Apr-24	10-Apr-24	With the new NEMA 23, the plates were installed the two days before DAID.

Cost/Budget

Our project budget was $1000, and we spent $1,037.34.

We found various ways to cut down costs of our project through in house machining and using recycled components from past projects. The majority of our mechanical parts were machined in house using the IGEN shop. While designing parts, we ensured that they could be manufactured in the shop so we could

avoid the use of vendors and the additional costs associated. We were able to use electrical components that we previously had, which cut down a lot of the smaller costs.

Our major costs came from parts that we were not able to manufacture ourselves. This includes the rack and pinion system, where the level of precision required was not attainable using our own manufacturing methods. The linear guide rails that we used for the sled testing were also ordered because a majority of the cost came from the raw materials used, and fabricating our own would not have cut down the price by a substantial amount. A full cost breakdown is included in Appendix D.

Responsibility Distribution

Table 4: Responsibility Distribution

Team Member	Role	Contributions
Lucas Petersen	Mechanical Design, feature integration	Prototyping, motor coding, stepper motor integration, mechanical design, manufacturing design, component and equipment sourcing
Arjav Prasad	Software, Electrical	Coding of esp32, build sensor circuit, setting up GitHub, considered use cases, prototyping, set up accelerometer setup, researched competition
Charlie Lever	Sensor System Design and Integration, Testing System Fabrication	Designing sensor system logic and code, Implementing sensor system into mechanical system, Building and Wiring Electrical System, Fabricating Test Rig
Kayla Butcher	Mechanical Design, Sensor Integration, Software/Code	Actuator Design, Mechanical Design, CAD, Fabrication of Prototype, Waterjet & CNC Manufacturing of parts, Drawings + CAD for final assembly
Ishaan Sareen	Integration,Design, Prototyping, Tester	Testing, Control System, Component sizing, Prototyping
Sena Akalp	Testing system design and implementation, sensor design, circuit wiring	Design and building of the testing system: the test dummy and the railing system. Setup and design of the sensors and their implementation, wiring and building of circuits, power and impulse time calculations.

Socio-Economic Design Assessment

Social Impact

The halo headrest system, designed to prevent whiplash injuries, brings significant social benefits, including improved safety, greater accessibility to advanced safety features, shifts in industry standards,

and better public awareness. By reducing the severity and frequency of whiplash injuries, the system not only enhances the well-being of vehicle occupants but also substantially decreases the number and cost of associated insurance claims. This reduction in claims can lead to lower insurance premiums for consumers.

Easily retrofitted onto existing vehicle seats, the system broadens access to these safety features, setting a new benchmark that may encourage industry-wide adoption and potentially initiate a shift in safety standards. Furthermore, it raises public understanding of the critical role headrest positioning plays in preventing injuries, potentially influencing consumer behavior and driving regulatory changes. This heightened awareness can lead consumers to prioritize safety features, exerting pressure on the automotive industry to continuously enhance safety standards.

Economic Impacts

The economic consequences of whiplash can be extensive from medical builds to effecting work output and salary over a lifetime. By preventing whiplash, users can reduce the risk of medical expenses, rehabilitation costs, and potential legal implications from accidents. Moreover, in the event of a chronic life-long injury, individuals can be affected by reduced work output and thus stagnation of wages or the inability to continue certain forms of labor.

Disposal Plans

Our team is committed to an environmentally sustainable, economically sustainable and responsible project lifecycle. The disposal plan for the headrest system is first the recycling of all 3D printed components using the 3D Print shop in IGEN. Secondly, all of the aluminum components will be donated back to the shop for future recycling into projects and into the scrap bin to be recycled. Lastly, all of the electrical components such as the stepper motors and ESP-32 are being taken home by members for future personal projects. The test dummy used was taken by Sena to be recycled.

Conclusions & Recommendations

In conclusion, the final design of our crash detection and head restraint adjustment system represents a sophisticated blend of technology and engineering, aimed at enhancing vehicle safety. The crash detection system cleverly combines LiDAR and acceleration sensing to predict and detect rear-end collisions. The use of the VL6180 LiDAR sensor at the vehicle's rear end and the MPU 6050 accelerometer provides a comprehensive system approach to collision detection as inspired by the Windsor Group. While the LiDAR sensor primarily serves as the early warning system, the accelerometer acts as a critical redundancy, ensuring functionality under varied light conditions and immediate crash detection.

The head sensing component, employing three VL6180 sensors, tracks the occupant's head position in both the X and Y directions. This precise tracking allows for the dynamic repositioning of the head restraint, which is crucial in mitigating neck injuries during collisions by eliminating the distance from the occupants head to the restraint. The integration of these sensors with the ESP32, despite the challenge of

their default I2C addresses, demonstrates a high level of innovation in system design and electronic integration.

Furthermore, the movement of the head restraint, facilitated by a telescoping actuator and a rack and pinion mechanism, ensures that the headrest can adjust both forward-backward and up-down with ease and precision. This multi-directional adjustability is vital for accommodating different occupant sizes and seating positions, thereby maximizing comfort and safety. The use of the NEMA 17 with integrated gearbox allows for our system to have lightweight, high-torque components.

Overall, this project not only showcases a high level of technical proficiency and innovative design but also reflects a deep commitment to enhancing vehicular safety. The detailed system drawings in the Appendix provide a comprehensive overview of this sophisticated safety solution.

For future iteration our team would recommend the use of a gearbox integrated stepper motor for the Y actuation as well as the X actuation to decrease weight and bulkiness of the system. The lighter the system, the more efficient the product and the easier it is to handle and ship if in a product situation. Similarly, by consolidating the motors to be the same component, this reduces the cost of manufacturing and assembly and eases the difficulty of sourcing. For the material of components, the current components made of aluminum have high manufacturability and dimensional accuracy but introduce bulk and weight into the system. Shifting the design into composite components and sandwich panels made of aluminum struts and carbon fibre panels would allow for weight elimination while keeping the strength of components. For design and innovation day we were showcasing the mechanical components but as a product would aim to have a carbon fibre shell for not only a sleek design, but pinching hazard mitigation. One component of the project which needed large improvement was the electrical wiring. This system was made of the wires in-house and lacked the proper harnessing or custom PCB to ensure the organization and reliability of the product.

References

[1]W. H. M. Castro, M. Schilgen, S. Meyer, M. Weber, C. Peuker, and K. Wörtler, "European Spine Society —The AcroMed prize for spinal research 1997," *European Spine Journal*, vol. 6, no. 6, pp. 366–375, Dec. 1997, doi: https://doi.org/10.1007/bf01834062.

[2]Z. Srp, M. Soucek, and K. Liptak, "ENGINEERING DESIGN OF HEADREST FOR PASSENGER MOTOR CAR," *Semantic Scholar*, 2005. https://www.semanticscholar.org/paper/ENGINEERING-DESIGN-OF-HEADREST-FOR-PASSENGER-MOTOR-Srp-Soucek/7d19456f7c8450f536316eb9efc4f733e81f565b (accessed Apr. 15, 2024).

Appendices

Appendix A - VL6180 vs. HC-SR04 Test

Figure X : VL6180 - Time of Flight Distance Sensor

Static Wall Test:

Both sensors are stationary and facing a blank wall to measure the consistency of distance readings. The image shows the distances over three readings.

```
HC-SR04 Distance: 34.47
VL6180 Lux: 3.84
VL6180 Range: 46
HC-SR04 Distance: 37.73
VL6180 Lux: 3.84
VL6180 Range: 46
HC-SR04 Distance: 33.61
VL6180 Lux: 3.84
VL6180 Range: 46
```

Figure A.1: Static Wall Test Results

Head Movement Test:

In this test, the sensors were stationary and tracking the distance of a head placed in front of them. The head moved side to side, in the lateral direction, and the distances were recorded. This test was done to examine the precision in field of view of each sensor, and the effect that a moving head has on the sensors. The VL6180 distance changed slightly with head movement, as expected. Whereas the HC-SR04 distance moved drastically in an unexpected pattern with head movement (e.g. changed from 170 mm to 22,000 mm to 1,200 mm with slight head movement). The setup for this test is shown below.
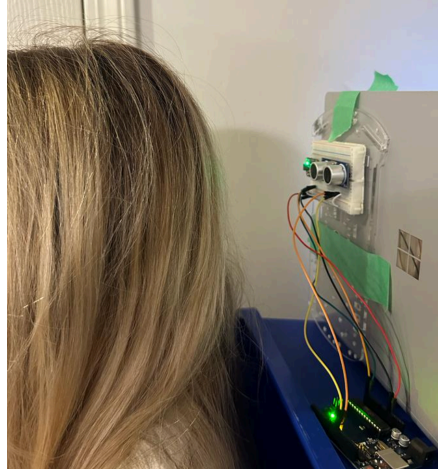
Figure A.2: Head Movement Test Setup

Hair Test:

The hair test was used to measure the effects of different hairstyles on each sensor. This test examined the measured distances when the hair was in a bun. The VL6180 showed a relatively consistent distance, whereas the HC-SR04 did not detect the hair or head and showed a distance of ~22,000 mm. The setup and results are shown below.
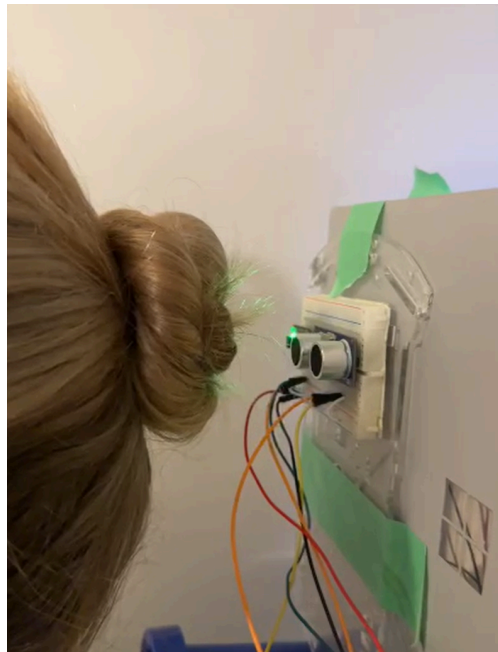
Figure A.3: Hair Test Setup
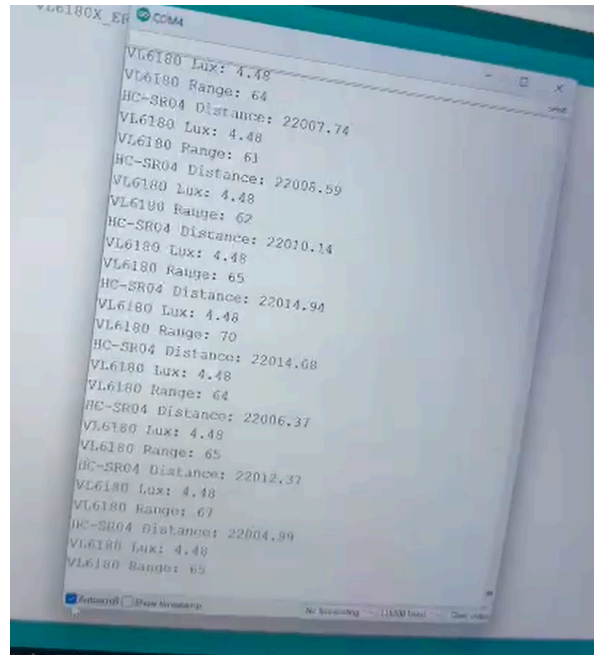
Figure A.4: Hair Test Results

Appendix B - Software

Link B.1: Link to project Github
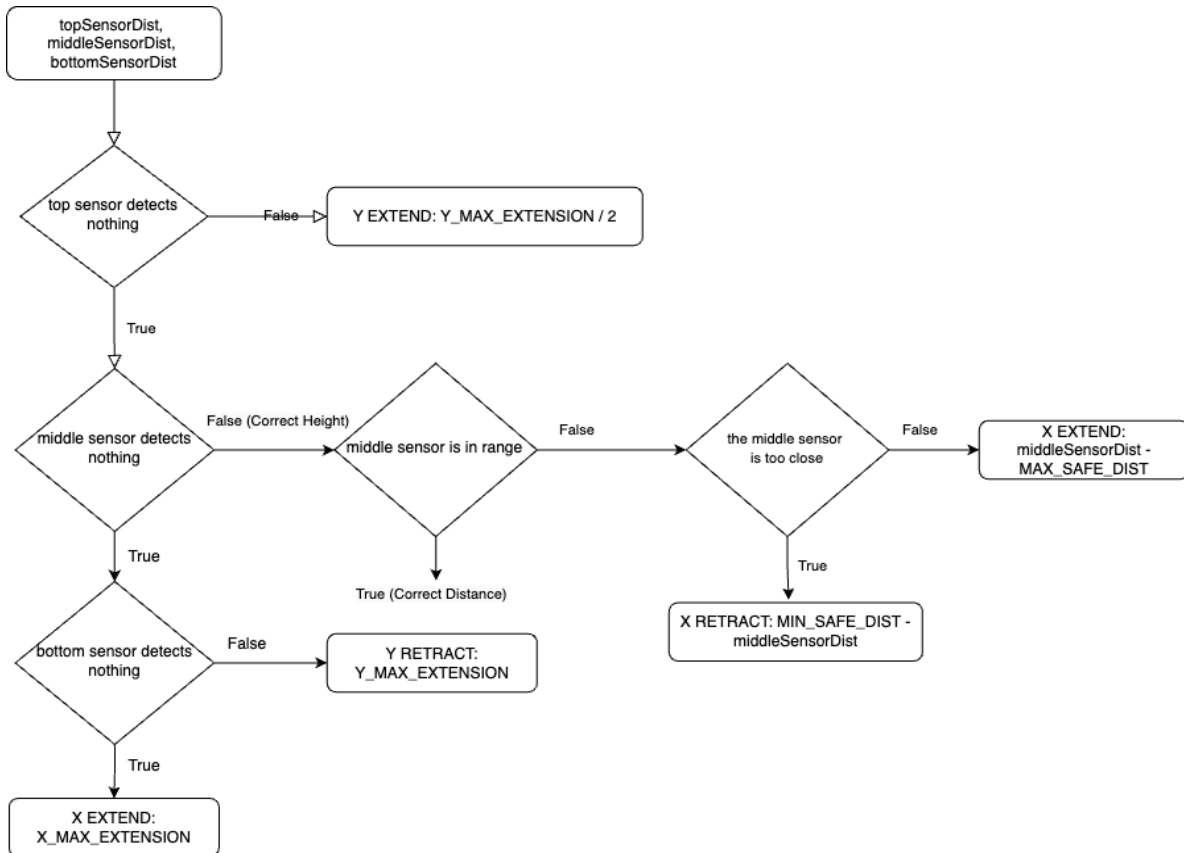
Figure B.1: Processing head position flowchart

Figure B.2: Serial output for headrest control program

```
//MOTOR Settings
//Microstep: 4
//Pulse/rev: 800
void actuateX(bool extend, int distance) {
  boolean motorPulseState = LOW;                                // pulse state
  int pulses = round((static_cast<float>(distance) / 60.0) * 800);  //distance (mm) * 60mm/1rev * 800 pulses/rev = pulses
  // Set the direction based on the extend parameter
  digitalWrite(X_MOTOR_DIR, extend ? LOW : HIGH);  // LOW for extending (CW), HIGH for retracting (CCW)

  for (int i = 0; i < pulses; i++) {
    motorPulseState = !motorPulseState;          // inverts the state of the variable
    digitalWrite(X_MOTOR_PUL, motorPulseState);  // assigns the new state to the port
    delayMicroseconds(motorPulseInterval);
  }
}

//MOTOR Settings
//Microstep: 4
//Pulse/rev: 800
void actuateY(bool extend, int distance) {
  boolean motorPulseState = LOW;                                // pulse state
  int pulses = round((static_cast<float>(distance) / 60.0) * 800);  //distance (mm) * 60mm/1rev * 800 pulses/rev = pulses
  // Set the direction based on the extend parameter
  digitalWrite(Y_MOTOR_DIR, extend ? LOW : HIGH);  // LOW for extending (CW), HIGH for retracting (CCW)

  for (int i = 0; i < pulses; i++) {
    motorPulseState = !motorPulseState;          // inverts the state of the variable
    digitalWrite(Y_MOTOR_PUL, motorPulseState);  // assigns the new state to the port
    delayMicroseconds(motorPulseInterval);
  }
}
```

Figure B.3: Motor Actuation Functions

Appendix C - Electrical
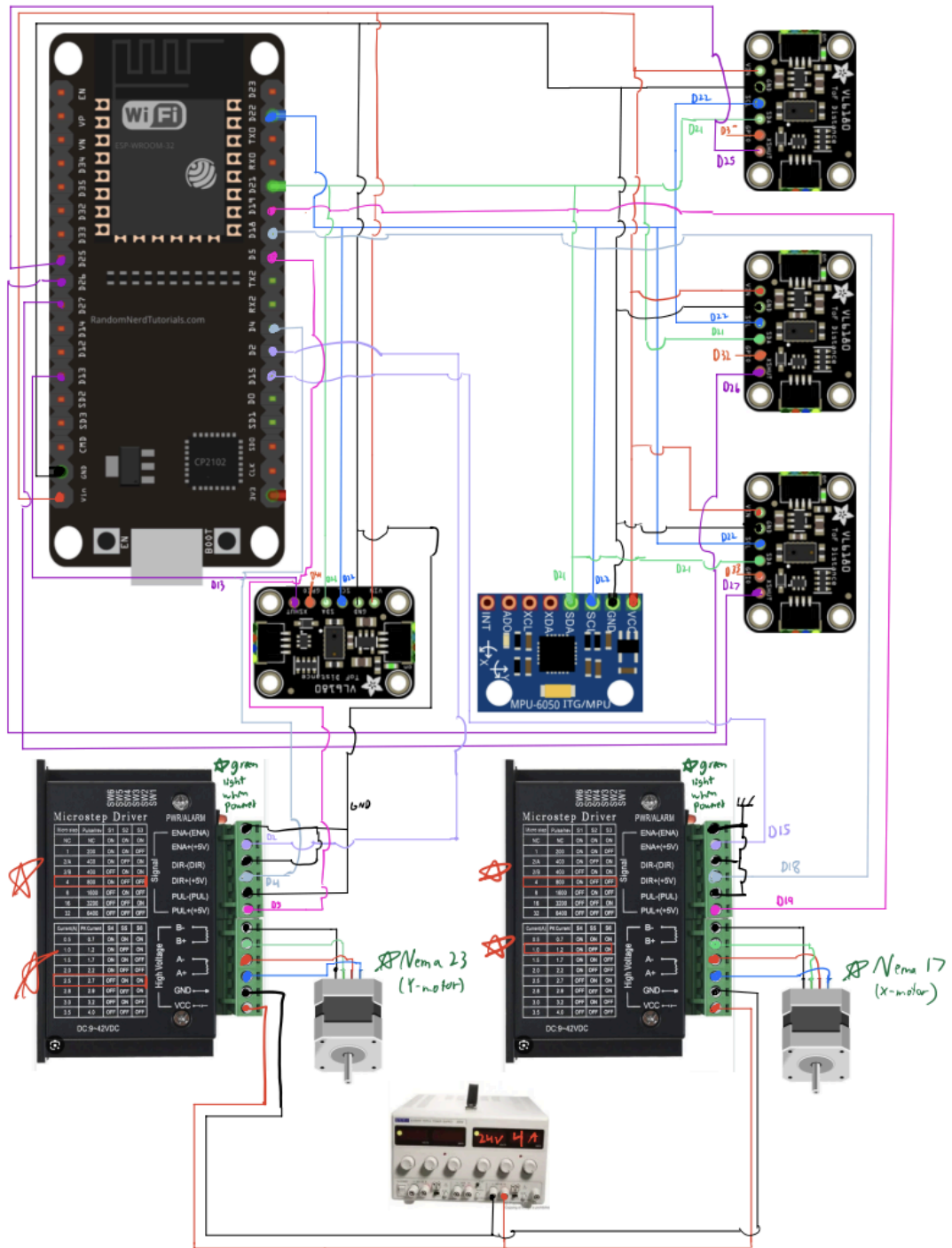
Figure C.1:Main System Circuit Diagram

HIGH TORQUE HYBRID STEPPING MOTOR SPECIFICATIONS

General specifications		Electrical specifications	
Step Angle (°)	1.8	Rated Voltage (V)	4
Temperature Rise (°C)	80 Max (rated current.2 phase on)	Rated Current (A)	1.2
Ambient temperature (°C)	-20~+50	Resistance Per Phase (±10%Ω)	3.3 (25°C)
Number of Phase	2	Inductance Per Phase (±20%mH)	2.8
Insulation Resistance	100MΩ, Min (500VDC)	Holding Torque (Kg.cm)	3.17
Insulation Class	Class B	Detent Torque (g.cm)	200
Max.radial force (N)	28 (20mm from the flange)	Rotor Inertia (g.cm²)	68
Max.axial force (N)	10	Weight (Kg)	0.365

● Wiring Diagram:

● Pull out torque curve:
VOLTAGE: 24VDC, CONSTANT CURRENT: 1.2A, HALF STEP

● Dimensions:
(unit=mm)
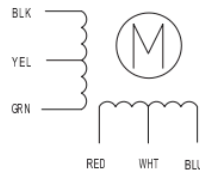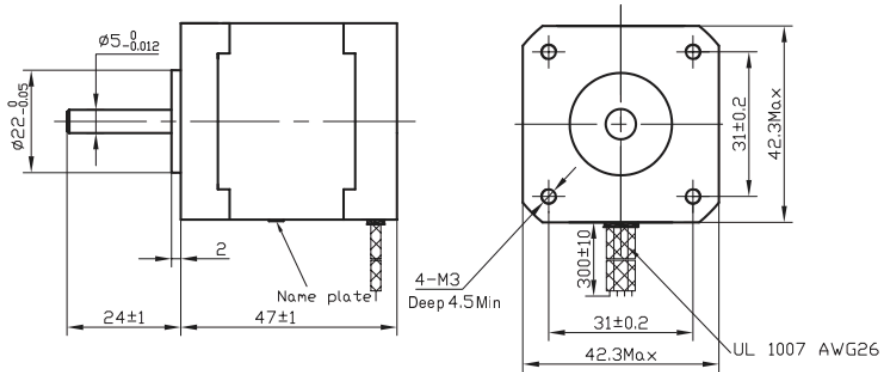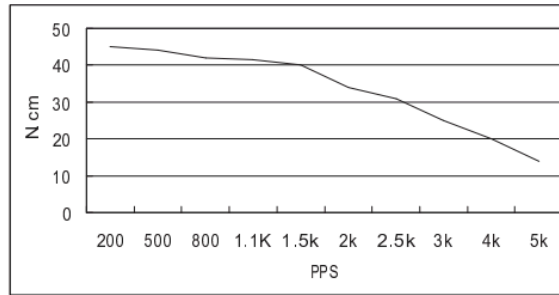
REV	REVISIONS	DESCRIPTION	BY	DATE	SY42STH47-1206A	TECHNICAL CONDITIONS
DRAW	任飞飞 2010.06.29					
CHECK					CHANGZHOU SONGYANG MACHINERY & ELECTRONICS NEW TECHNIC INSTITUTE	060047000
APPROVE						

Figure C.2: NEMA 17 Motor Specifications Sheet

HIGH TORQUE HYBRID STEPPING MOTOR SPECIFICATIONS

General specifications		Electrical specifications	
Step Angle (°)	1.8	Rated Voltage (V)	3.2
Temperature Rise (℃)	80 Max (rated current、2 phase on)	Rated Current (A)	2.8
Ambient Temperature (℃)	-20~+50	Resistance Per Phase (±10% Ω)	1.13
Number of Phase	2	Inductance Per Phase (±20% mH)	3.6
Insulation Resistance (MΩ)	100 Min (500VDC)	Holding Torque (N.cm)	189
Insulation Class	Class B	Weight (Kg)	1.05
Max.radial force (N)	75 (20mm from the flange)		
Max.axial force (N)	15		

● Wiring Diagram :
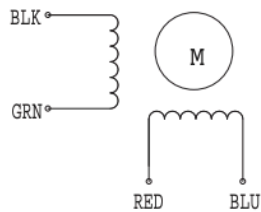
● Pull out torque curve :

VOLTAGE: 30VDC, CONSTANT CURRENT:2.8A,HALF STEP

● Dimensions:

(unit=mm)
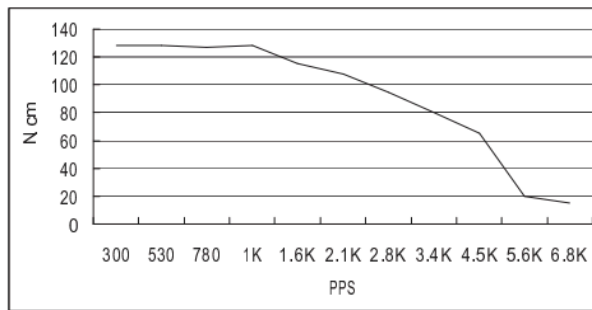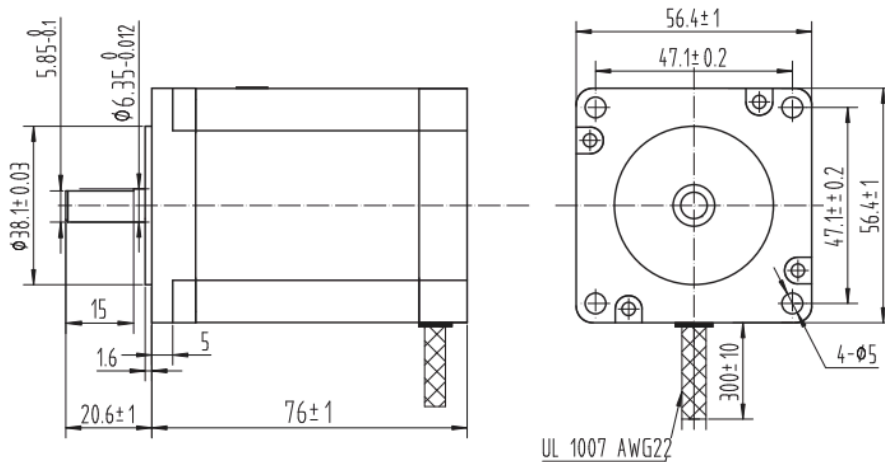
REV	REVISIONS	DESCRIPTION	BY	DATE	SY57STH76-2804A	TECHNICAL CONDITIONS
DRAW	kongxiangzhen 2012.05.16				CHANGZHOU SONGYANG MACHINERY & ELECTRONICS	
CHECK					NEW TECHNIC INSTITUTE	080076026
APPROVE						

Figure C.2: NEMA 23 Motor Specifications Sheet

Appendix D - Cost Breakdown

Whiplash - Expense Report

09/01/23 - 04/11/24

Date	Category	Description	Status	Name and Notes	Amount
10/12	Hardware	Car seat	Delivered	Kayla	$0.00
10/15	Electronics	Arduino Uno 2x	Delivered	AP	$0.00
10/20	Electronics	Transistor ULN-2004 Array	Delivered	Lucas	$6.00
10/23	Electronics	Timing Motor Pulley + Stepper Motor	Delivered	Lucas	$28.00
11/3	Electronics	VL6180 ToF Sensor x4	Delivered	Charlie	$91.88
11/9	Electronics	ESP-32	Delivered	Ishaan	$13.00
11/9	Electronics	MPU-6050	Delivered	Ishaan	$14.00
11/25	Mechanical	98mm Aluminum RC Shock Absorber	Delivered	Lucas	$22.38
12/7	Electronics	Luna LiDAR	Delivered	Ishaan	$36.00
1/21	Hardware	Mannequin	Delivered	Sena	$50.00
1/31	Electronics	FSRs	Delivered	Ishaan	$32.00
1/30	Mechanical	Springs x11	Delivered	Sena	$23.68
2/6	Mechanical	NEMA 23 Stepper	Ordered	Lucas	$39.19
3/7	Hardware	Gravel	Delivered	Sena	$9.49
3/8	Hardware	Stepper motor driver x2	Delivered	Charlie	$47.04
3/18	Hardware	Stepper motor	Delivered	Lucas	$13.43
3/18	Hardware	Ball Bearings	Delivered	Lucas	$11.19
3/14	Mechanical	Linear guide rails 1	Delivered	Charlie	$86.23
3/18	Mechanical	Linear guide rail 2	Delivered	Charlie	$91.83
3/19	Mechanical	Foam	Picked up	Lucas	$19.43
2/14	Mechanical	McMaster Order	Delivered	Lucas	$343.24
3/25	Electronics	TB6600 Stepper Motor Driver	Delivered	AP	$42.54
3/26	Mechanical	Drag Chain Cable Carrier	Delivered	Lucas	$16.79

$1,037.34

Appendix E - Testing and Validation

Figure E.1: Final Sled Assembly
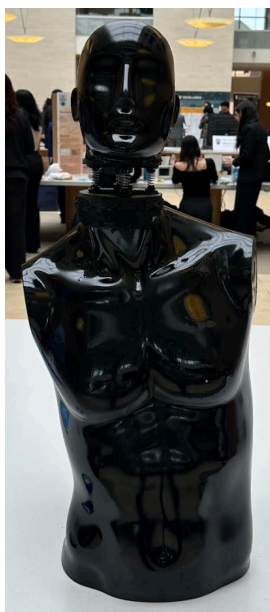
Figure E.2: Front View of Crash Test Dummy

Figure E.3: Side View of Crash Test Dummy

Figure E.4: Artificial Neck
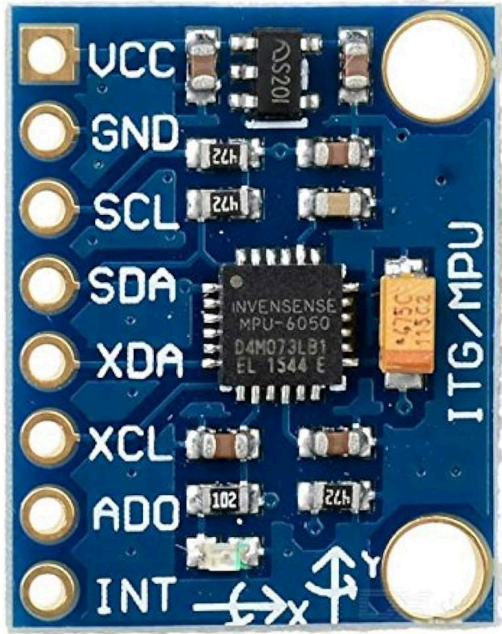
Figure E.5: MPU 6050
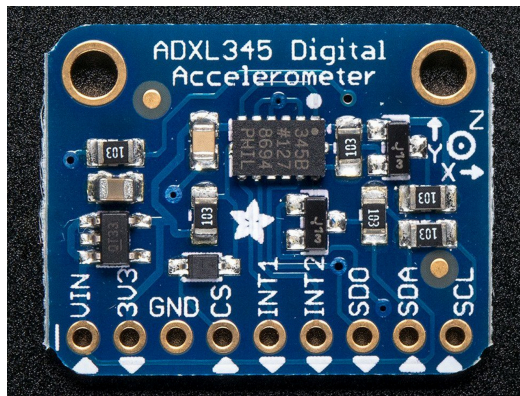
Figure E.6: ADXL 345
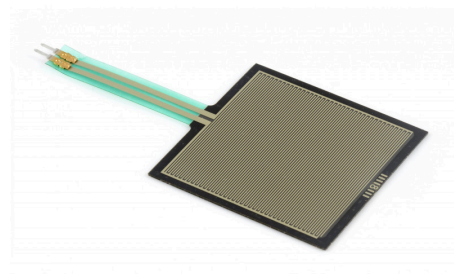
Figure E.7: Square FSR

```
#include <ArduinoIoTCloud.h>
#include <Arduino_ConnectionHandler.h>

const char DEVICE_LOGIN_NAME[]  = "a365d09d-c757-4639-aef6-3f2e1d6ad04d";

const char SSID[]               = SECRET_SSID;    // Network SSID (name)
const char PASS[]               = SECRET_OPTIONAL_PASS;    // Network password (use for WPA, or use as key for WEP)
const char DEVICE_KEY[]  = SECRET_DEVICE_KEY;    // Secret device password


float a2x;
float a2y;
float a2z;
float accelX;
float accelY;
float accelZ;
int forceSensor1Value;
int forceSensor2Value;

void initProperties(){

  ArduinoCloud.setBoardId(DEVICE_LOGIN_NAME);
  ArduinoCloud.setSecretDeviceKey(DEVICE_KEY);
  ArduinoCloud.addProperty(a2x, READ, 1 * SECONDS, NULL);
  ArduinoCloud.addProperty(a2y, READ, 1 * SECONDS, NULL);
  ArduinoCloud.addProperty(a2z, READ, 1 * SECONDS, NULL);
  ArduinoCloud.addProperty(accelX, READ, 1 * SECONDS, NULL);
  ArduinoCloud.addProperty(accelY, READ, 1 * SECONDS, NULL);
  ArduinoCloud.addProperty(accelZ, READ, 1 * SECONDS, NULL);
  ArduinoCloud.addProperty(forceSensor1Value, READ, 1 * SECONDS, NULL);
  ArduinoCloud.addProperty(forceSensor2Value, READ, 1 * SECONDS, NULL);

}

WiFiConnectionHandler ArduinoIoTPreferredConnection(SSID, PASS);
```

Figure E.9: Testing Program
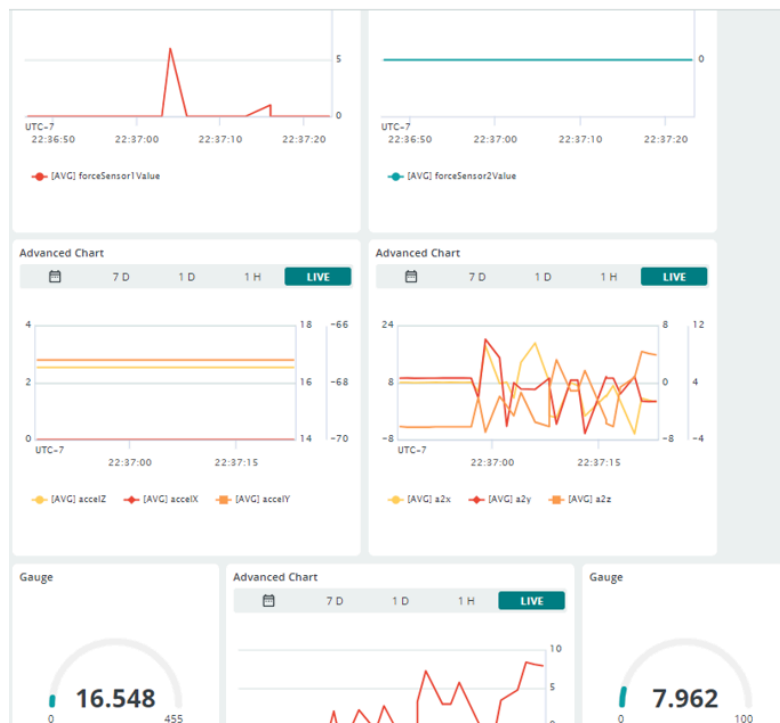
Figure E.10: Completed Dashboard
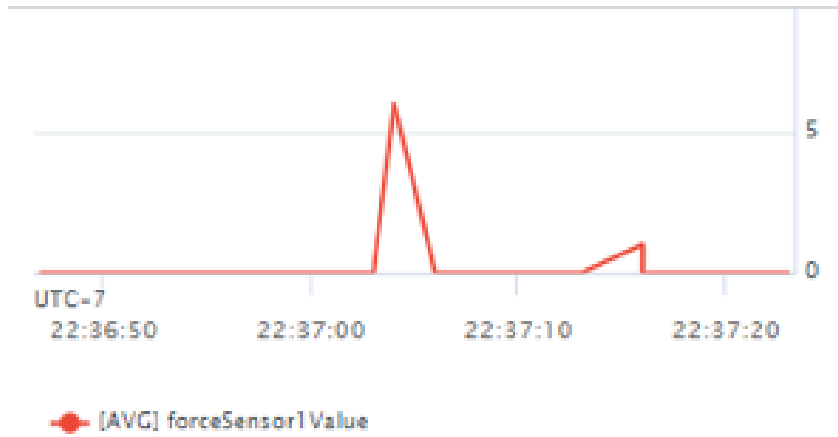
Figure E.11: Head Impact Detection
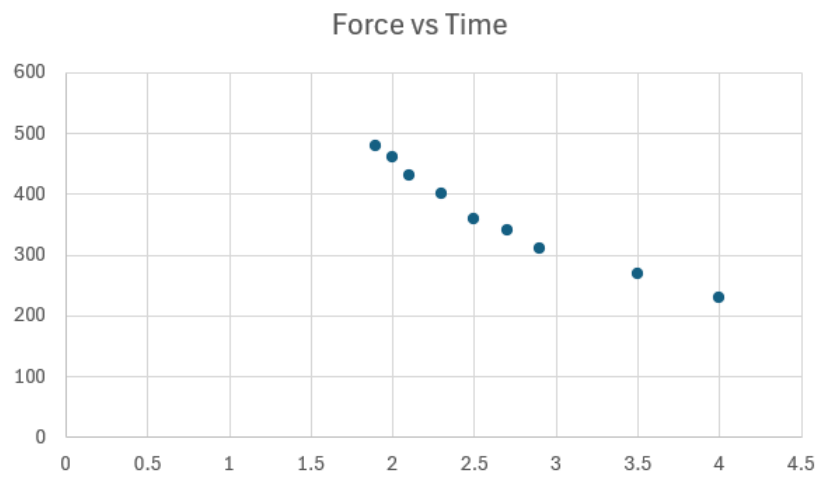
Figure E.12: Measurement of Force Response and Impulse

$\Delta t_1 = 1.2$
$\Delta t_2 = 1$
$\Delta t_3 = 0.7$
$\Delta t_4 = 1$
$\Delta t_5 = 0.8$
$\Delta t_6 = 0.8$
$\Delta t_7 = 1.3$
$\mathbf{\Delta t_{Average} < 1\ second}$

Figure E.13: Response Time Trials

Appendix F - Mechanical Calculations

430 - Capstone - Whiplash — Mechanical Calculations

Parameters

Mechanical

Average Force		
Maximum Force	890	N
Average Moment		
Maximum Moment	372	Nm
Maximum Deflection under	100	mm
Speed of Travel	12	mph

Electrical

System Voltage	12	V
Run time		
Allowable Temp	40	C

Regulations (NHTSA)

During a forward acceleration of at least 8g on the seat supporting structure, the rearward angular displacement of the head reference line shall be limited to 45° from the torso reference line

Head restraints must be at least 700 mm (27.6 in) above the seating reference point in their highest position and not deflect more than 100 mm (3.9 in) under a 372 N·m (3,292 in·lbf) moment. The lateral width of the head restraint, measured at a point either 65 mm (2.56 in) below the top of the head restraint or 635 mm (25.0 in) above the seating reference point must be not less than 254 mm (10.0 in) for use with bench seats and 171 mm (6.73 in) for use with individual seats. The head restraint must withstand an increasing rearward load until there is a failure of the seat or seat back, or until a load of 890 N (200 lbf) is applied.

Telescoping Actuator (Impact)

Material	Tough Resin	
Area 1	103.12	mm
Area 2	277.87	mm
Area 3	567.5	mm
Area 4	676.64	mm
Area 5	781.23	mm
Minimum Area	103.12	mm
Safety Factor	1.75	
Force	890	
Normal Stress	15.10376261	N/mm (M
Allowable Stress	33	Mpa
σ < σ allowable?	Yes	
Impact IZOD	1387	J/m <-
Impact Velocity	5.363333333	mps <-
Impact Energy	1258.483819	J/m <-
Impact < Allowable Impact?	Yes	
Compact Length	43	mm
Extended Length	105.54	mm
%Extension	145%	mm

Bus Bar Fatigue (TN Curve)

Cycle		
Temperature		C
Stiffness		
Deflection	9.19E-05	

Figure F.1: Parameters, Telescoping Actuator Calculations

Motor Sizing (X-Direction)		
System Voltage	12 V	
Weight of Load	0.804 kg	<-- Weight of Foam, Plates, Sensors, Actuator
Friction Co-efficient	0.3	<-- Nylon, Nylon
Diameter	15 mm	<-- Diameter of lead screw
Length Actuator	105.54 mm	<-- Extended Length
Lead (Pitch)	55 mm/rev	<-- Helix Gear Pitch
Efficiency	0.7	
Material	Nylon	
Static Friction Coefficient	0.3	
Force	267	<-- Normal Force*Lead Diameter/2pi
Diameter (1)	15 mm	Force = Static Friction Coeff*Normal Force
Breakaway Torque (1)	0.63742 Nm	<-- Lead Screw
Diameter (2)	19.6 mm	
Breakaway Torque (2)	0.83289 Nm	<-- Secondary Screw
Total Breakaway Torque	1.47031 Nm	
External Force	890 N	
Stopping Accuracy	5 mm	
Positioning Distance	62.54 mm	<-- Extended Length - Compressed Length
Stopping Time	0.2 s	<-- Deceleration
Operational time	0.8 s	<-- Time for Extension
Safety Factor	1.75	
Results		
Load Inertia (Jw)	6.161E-05 kgm^2	
Load Inertia (Js)	5.770E-07 kgm^3	
Load Inertia (JL)	6.218E-05 kgm^4	
Required Speed	113.71 rpm	
Required Torque	25.0324 Nmm	
RMS Torque	27.545 Nmm	
Acceleration Torque	4.442E-03 Nmm	
Load Force	892.36 N	
Load Torque	12.245 Nmm	
Stopping Accuracy (Deg)	32.727 Degrees	
Other Requirements		
Electromagnetic Break?	Yes	<-- Select From Drop Down
Holding Torque	Yes	
Motor speed	**113.71** rpm	
Continuous Operation Torque	**3544.86** inch-oz	<-- McMaster Units

Figure F.2: Motor Sizing Calculations (X Direction)

Damper Sizing		
Mass	5	kg
Velocity	12	mph
Force	890	N
Displacement	100	mm
Velocity	5.36	m/s
# of Dampers	2	
Safety Factor	1.75	
Total Energy Capacity	71.940	
Total Energy Capacity (w/ SF)	125.895029	
Energy Capacity / Damper	62.948	Nm	<-- From 1/2mv^2 of head movement in 12mph impact
Energy Capacity / Damper	77.875	Nm	<-- From Allowable Force/Deflection

Figure F.3: Damper Calculations

Electrical Calculations

Bus Bar Sizing			
Material	Copper		
Resistivity	1.77E-08	ohm-meter	
Voltage	12	V	
Length	44.4	mm	<-- This is for the worst case
Width	3.5	mm	scenario (longest length,
Height	0.5	mm	highest resistance)
Cross Sectional Area	0.00000175	m^2	
Contact Resistance	0.007	m^2K/w	<-- from paper by NJIT
Rcontact	10000	ohms	<-- 1/(contact resistance coeff *A)
Sensor Wattage	350	mW	<-- lidar sensor
Current Required	29.167	mA	
Qin	3.8203E-07		<-- i^2*R, where $R = (\rho * L) / Area$
R	0.00044907		<-- $R = (\rho * L) / Area$
Temp Allowable	40	C	
Qout	0.002		<-- $Q = \Delta T/Rcontact$
Qout > Qin	Yes		<-- Check that copper does not exceed allowable heat

e seat
ent of the
e torso

Figure F.4: Electrical Calculations 1

Heat Generation (Qin)	Q =I^2*R			
Heat Generation (Qin) -- Time Dependen	Q =I^2*R*t			
Resistance of Wire	R=ρ*L/Area			
Resistivity, ρ	Given by Material			
Length, L	Given by Wire			
Area, Cross Sectional to Flow of Elec	Solving for area			
Heat Generation (Qin)	Q =I^2*(ρ*L/A)			
Heat Removed (Qout)	Q=Qconduction+Qradiation+Qconvection			
Qconduction (Circular Wire)	Qcd=2*pi*K*L*ΔT/ln(ro-ri)			
Qconvection	Qcv=h*2pi*L*ΔT			
Qradiation	Qr=			
Set Qin equal to Qout --> solve for area				
Example:				
I^2*(ρ*L/A) = h*2pi*L*ΔT	Exposed wire, no insulation			
I^2*(ρ*L/(pi*r^2)) = h*2pi*L*ΔT				
I^2*(ρ*L̶/(pi*r^2)) = h*2p̶i̶*L̶*ΔT				
r=(I^2)*(ρ)/(2h*ΔT)	solve for radius of wire			

Figure F.4: Electrical Calculations 2

MATLAB Script for Foam Deflection & Energy Absorption:

```
% Foam properties based on McMaster rating to compress 25%
% Calculate three different ratings for foam
% Foams considered 5 psi, 15 psi, 25psi
A_pressure_psi = 5; % example pressure in psi
A_pressure_Pa = A_pressure_psi * 6894.76; % converting psi to Pa
B_pressure_psi = 15; % example pressure in psi
B_pressure_Pa = B_pressure_psi * 6894.76; % converting psi to Pa
C_pressure_psi = 25; % example pressure in psi
C_pressure_Pa = C_pressure_psi * 6894.76; % converting psi to Pa
D_pressure_psi = 1; % example pressure in psi
D_pressure_Pa = D_pressure_psi * 6894.76; % converting psi to Pa
strain = 0.25; % 25% compression
% Calculating Young's Modulus
A_youngs_modulus_Pa = A_pressure_Pa / strain; % Young's modulus in Pascals
% Calculating Young's Modulus
B_youngs_modulus_Pa = B_pressure_Pa / strain; % Young's modulus in Pascals
% Calculating Young's Modulus
C_youngs_modulus_Pa = C_pressure_Pa / strain; % Young's modulus in Pascals
% Calculating Young's Modulus
D_youngs_modulus_Pa = D_pressure_Pa / strain; % Young's modulus in Pascals
```

```matlab
% Convert Young's modulus to MPa
A_youngs_modulus_MPa = A_youngs_modulus_Pa / 1e6; % 1 MPa
B_youngs_modulus_MPa = B_youngs_modulus_Pa / 1e6; % 1 MPa
C_youngs_modulus_MPa = C_youngs_modulus_Pa / 1e6; % 1 MPa
D_youngs_modulus_MPa = D_youngs_modulus_Pa / 1e6; % 1 MPA
initial_thickness = 50.8; % Initial thickness of the foam in mm
% Area over which the load is spread
length = 180; % length in mm
width = 180; % width in mm
area = length * width; % area in mm^2
% Load values from 0N to 850N
load_values = linspace(0, 850, 100); % 100 linearly spaced values
% Calculate stress, strain, and deflection for each load value
stress = load_values / area; % Stress in MPa (since 1 N/mm^2 = 1 MPa)
A_strain = stress / A_youngs_modulus_MPa; % Strain A (dimensionless)
B_strain = stress / B_youngs_modulus_MPa; % Strain B (dimensionless)
C_strain = stress / C_youngs_modulus_MPa; % Strain C (dimensionless)
D_strain = stress / D_youngs_modulus_MPa; % Strain C (dimensionless)
A_deflection = A_strain * initial_thickness; % Deflection in mm
B_deflection = B_strain * initial_thickness; % Deflection in mm
C_deflection = C_strain * initial_thickness; % Deflection in mm
D_deflection = D_strain * initial_thickness; % Deflection in mm
% Initialize energy_absorbed arrays with zeros
energy_absorbed_A = zeros(1, 100);
energy_absorbed_B = zeros(1, 100);
energy_absorbed_C = zeros(1, 100);
energy_absorbed_D = zeros(1, 100);
% Calculate energy absorbed for each load value for each foam
for i = 1:100
    stress_i = stress(i); % Current stress value in MPa
    % Energy absorbed for Foam A
    strain_A_i = A_strain(i); % Current strain for Foam A
    energy_absorbed_A(i) = 0.5*stress_i*strain_A_i*area*1e-3;
    % Energy absorbed for Foam B
    strain_B_i = B_strain(i); % Current strain for Foam B
    energy_absorbed_B(i) = 0.5*stress_i*strain_B_i*area*1e-3;
    % Energy absorbed for Foam C
    strain_C_i = C_strain(i); % Current strain for Foam C
    energy_absorbed_C(i) = 0.5*stress_i*strain_C_i*area*1e-3;

    % Energy absorbed for Foam D
    strain_D_i = D_strain(i); % Current strain for Foam C
    energy_absorbed_D(i) = 0.5*stress_i*strain_D_i*area*1e-3;
end
% Plotting the deflection vs. load
figure;
subplot(2,1,1); % Subplot for deflection (upper plot)
plot(load_values, A_deflection, 'b-', 'LineWidth', 2);
hold on;
```

```
plot(load_values, B_deflection, 'g-', 'LineWidth', 2);
plot(load_values, C_deflection, 'r-', 'LineWidth', 2);
plot(load_values, D_deflection, 'm-', 'LineWidth', 2);
hold off;
title('Deflection of Foam Under Load');
xlabel('Load (N)');
ylabel('Deflection (mm)');
legend('Foam A - Low Stiffness', 'Foam B - Medium Stiffness', 'Foam C - High Stiffness','Foam D - Ultra Low Stiffness');
grid on;
% Plotting the energy absorbed vs. load
subplot(2,1,2); % Subplot for energy absorbed (lower plot)
plot(load_values, energy_absorbed_A, 'b-', 'LineWidth', 2);
hold on;
plot(load_values, energy_absorbed_B, 'g-', 'LineWidth', 2);
plot(load_values, energy_absorbed_C, 'r-', 'LineWidth', 2);
plot(load_values, energy_absorbed_D, 'm-', 'LineWidth', 2);
hold off;
title('Energy Absorbed by Foam Under Load');
xlabel('Load (N)');
ylabel('Energy Absorbed (Nmm)');
legend('Energy Absorbed - Foam A', 'Energy Absorbed - Foam B', 'Energy Absorbed - Foam C', 'Foam D - Ultra Low Stiffness');
grid on;
```

Appendix G: CAD & Simulations
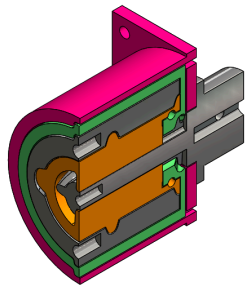
Figure: Split View Section (Compressed)
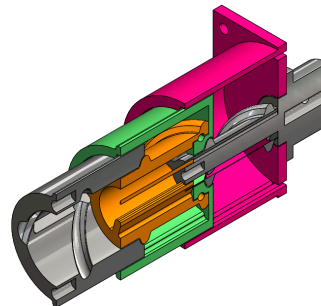
Figure: Split View Section (Extended)

Figure G-1: Simulation of Backplate

Figure G-2: Simulation of Backplate

Figure G-3: Simulation of Backplate

Figure G-4: Simulation of Backplate

Figure G-5: Simulation of Foam Stress

Figure G-6: Simulation of Backplate

Figure G-7: Simulation of Mounting Pins Deflection

Figure G-8: Simulation of Mounting Pins
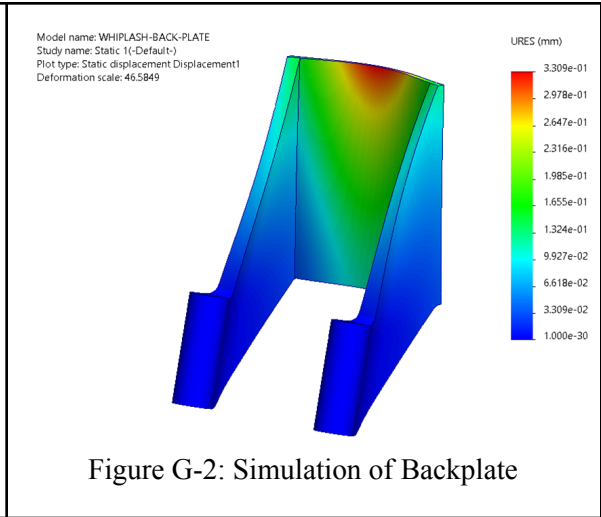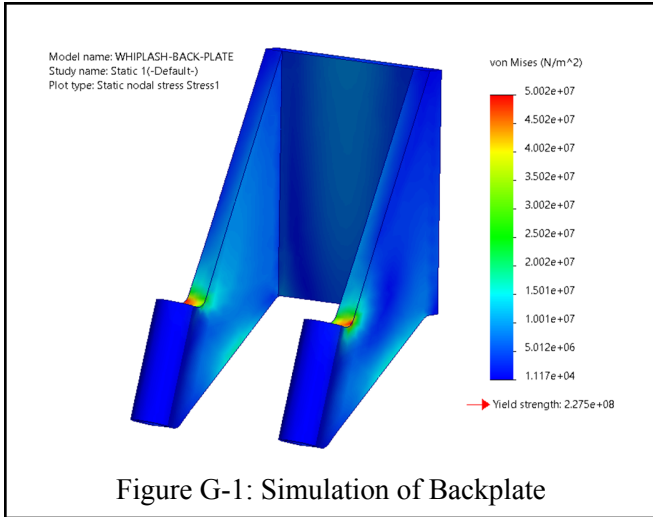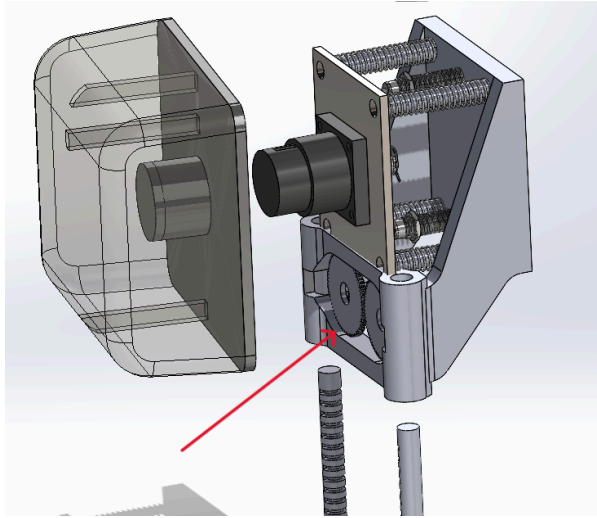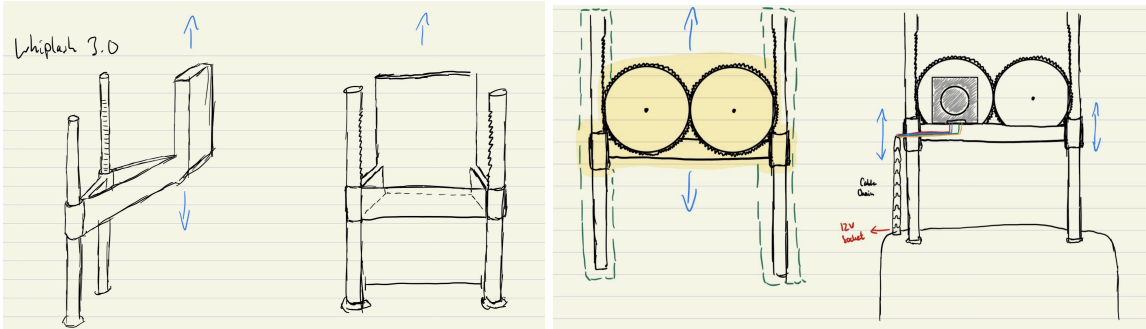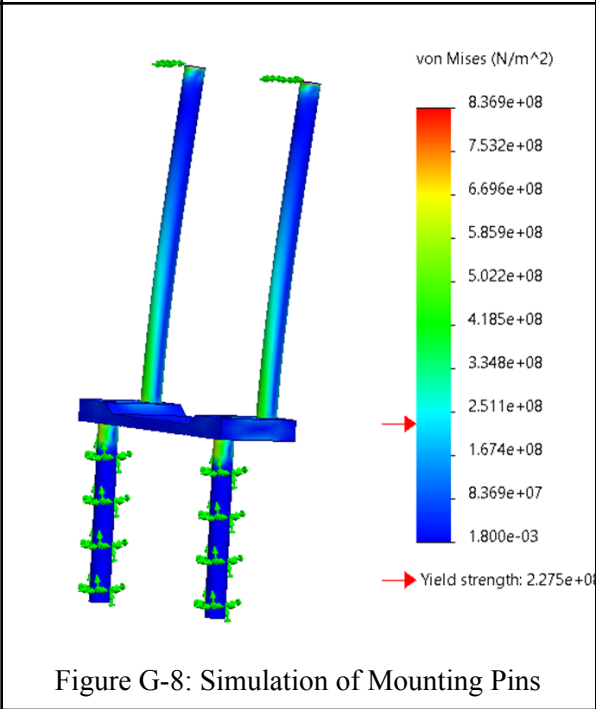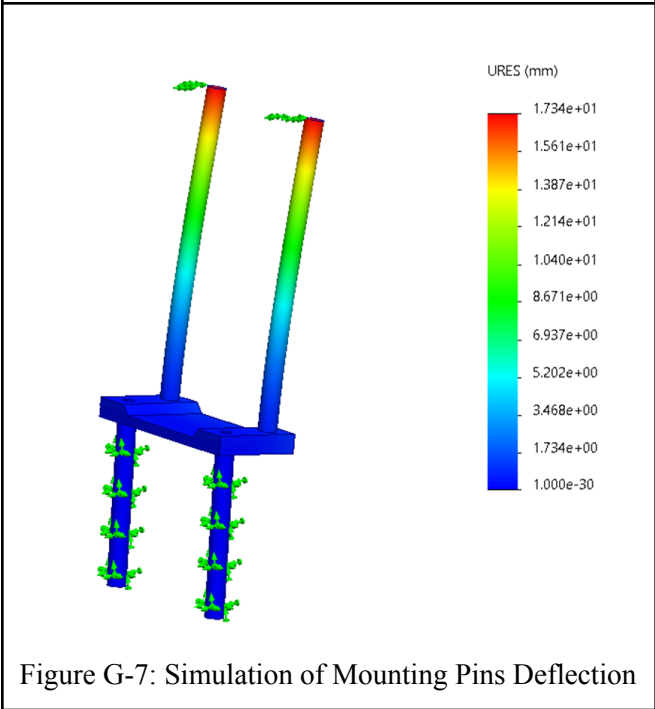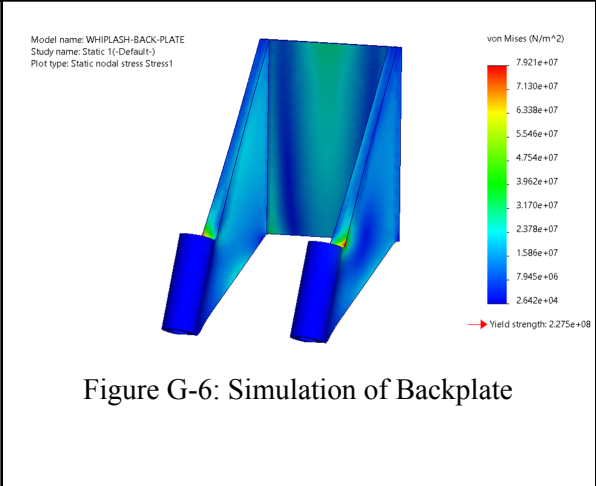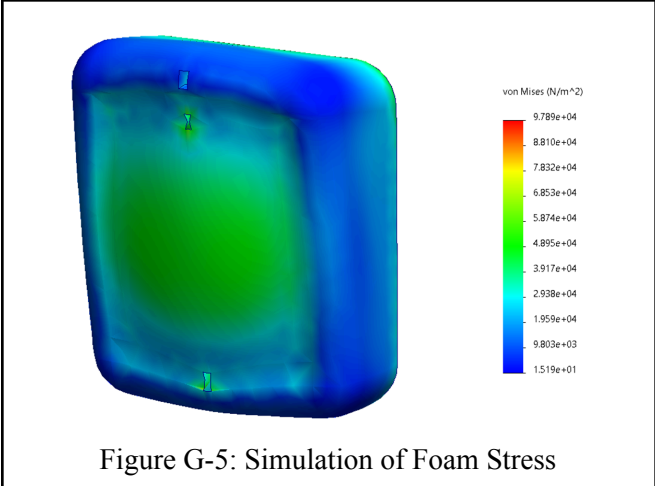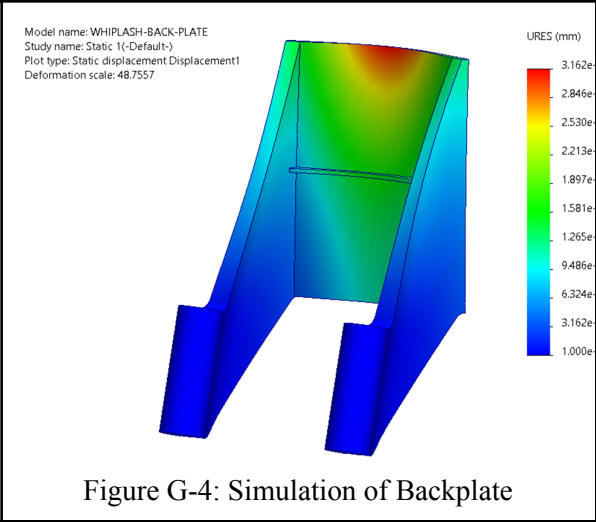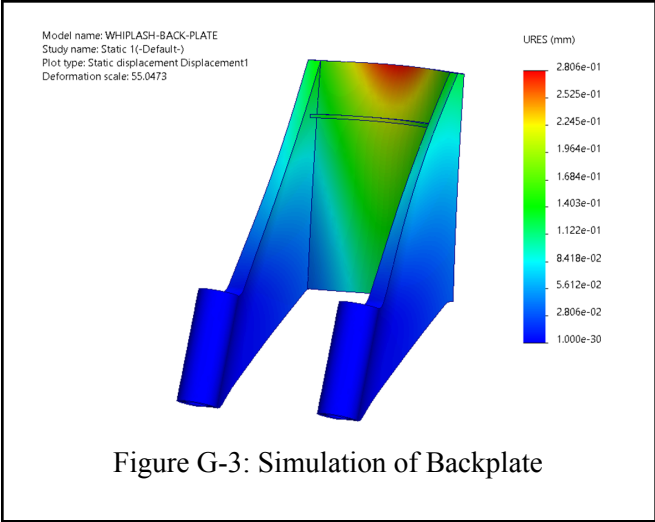
Appendix H: Technical Drawings

ITEM NO.	PART NUMBER	DESCRIPTION	QTY.
1	WHIPLASH-PIN-FRAME	PINS	1
2	WHIPLASH-MOVEMENT-PLATE	STEEL MOVEMENT PLATE	1
3	WHIPLASH-GUIDE-RAILS	GUIDE RAILS	4
4	9657K34	Compression Spring	4
5	6331K86_Compact Round-Face DC Motor	Compact Round-Face DC Motor	1
6	WHIPLASH-HEADREST-FOAM-INSERT	FOAM INSERT	1
7	WHIPLASH-BACK-PLATE	BACK PLATE	1
8	WHIPLASH-LIDAR-PCB	LIDAR PCB	3
9	WHIPLASH-SUPPORT-ROD	SUPPORT ROD	1
10	WHIPLASH-HEADREST-FOAM-BACK-PLATE	FOAM INSERT BACK PLATE	1
11	TELESCOPING-ACTUATOR-2.0	TELESCOPING ACTUATOR	1

Figure H-1: Exploded View - System Overview
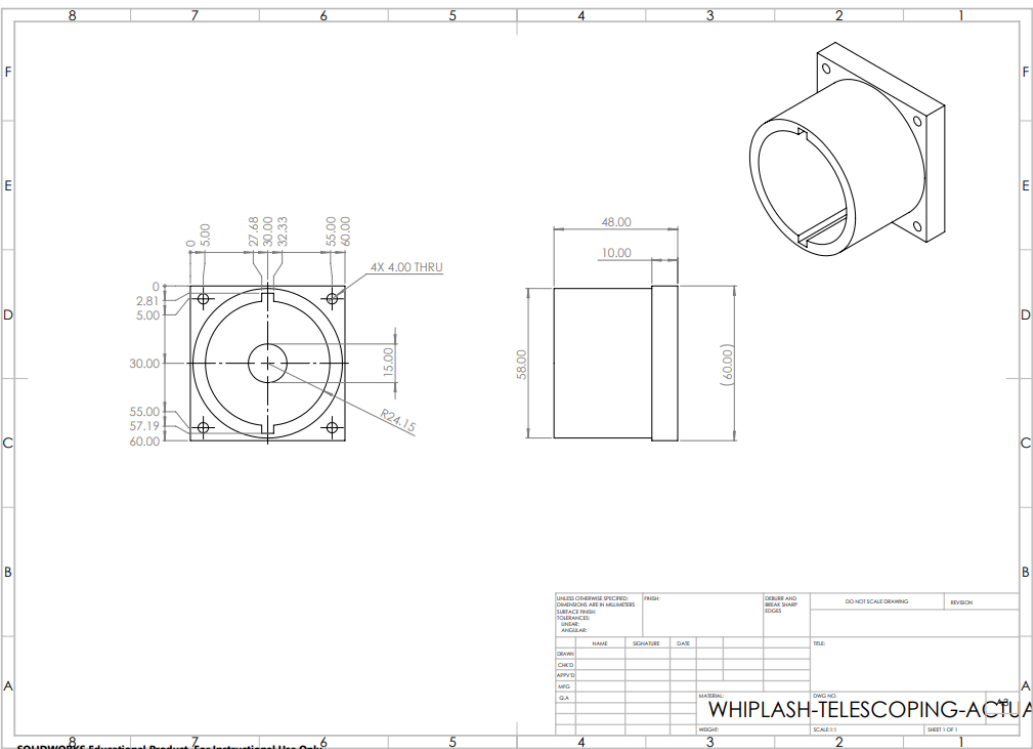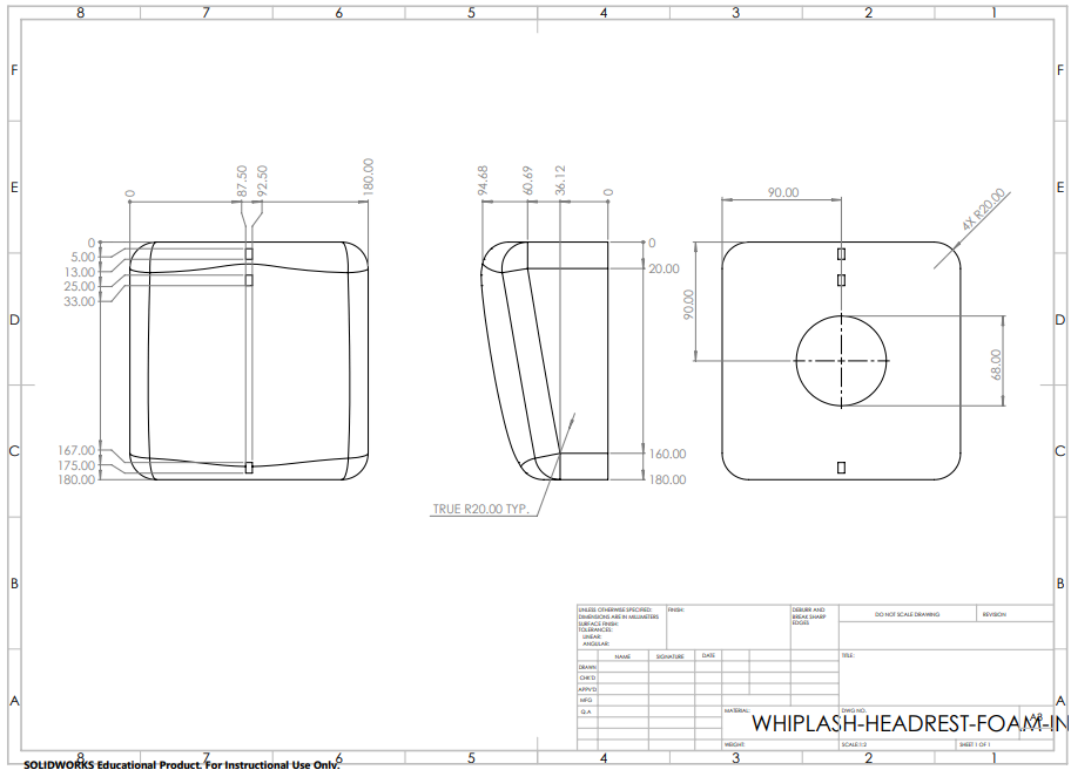

Figure H-2: Telescoping Actuator Base

Figure H-3: Foam Insert

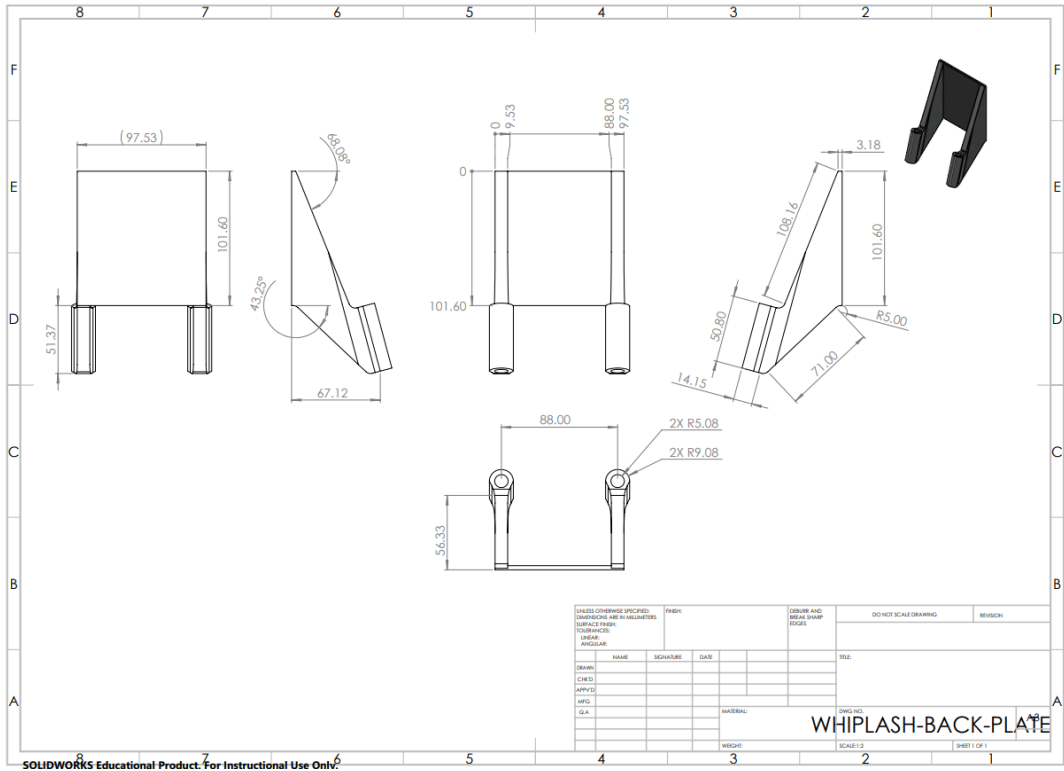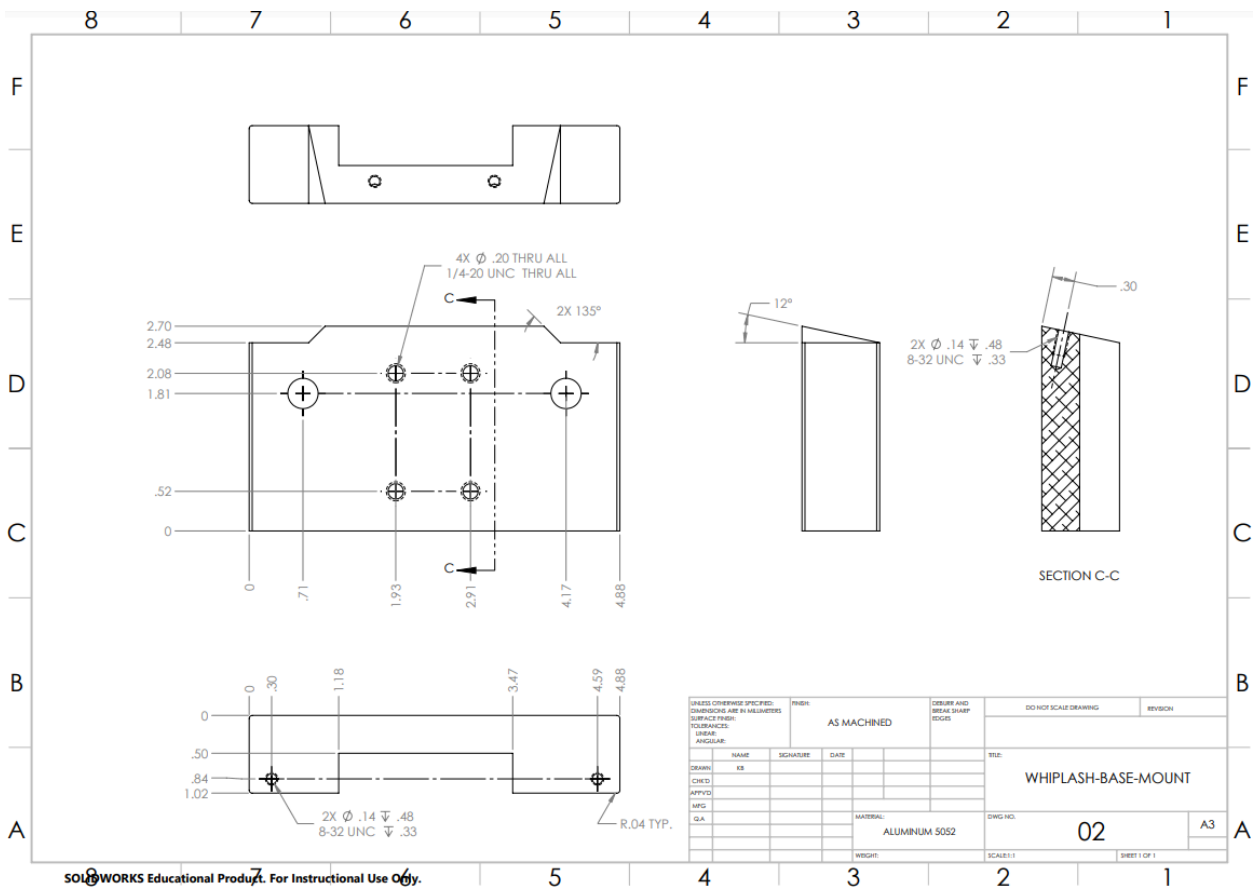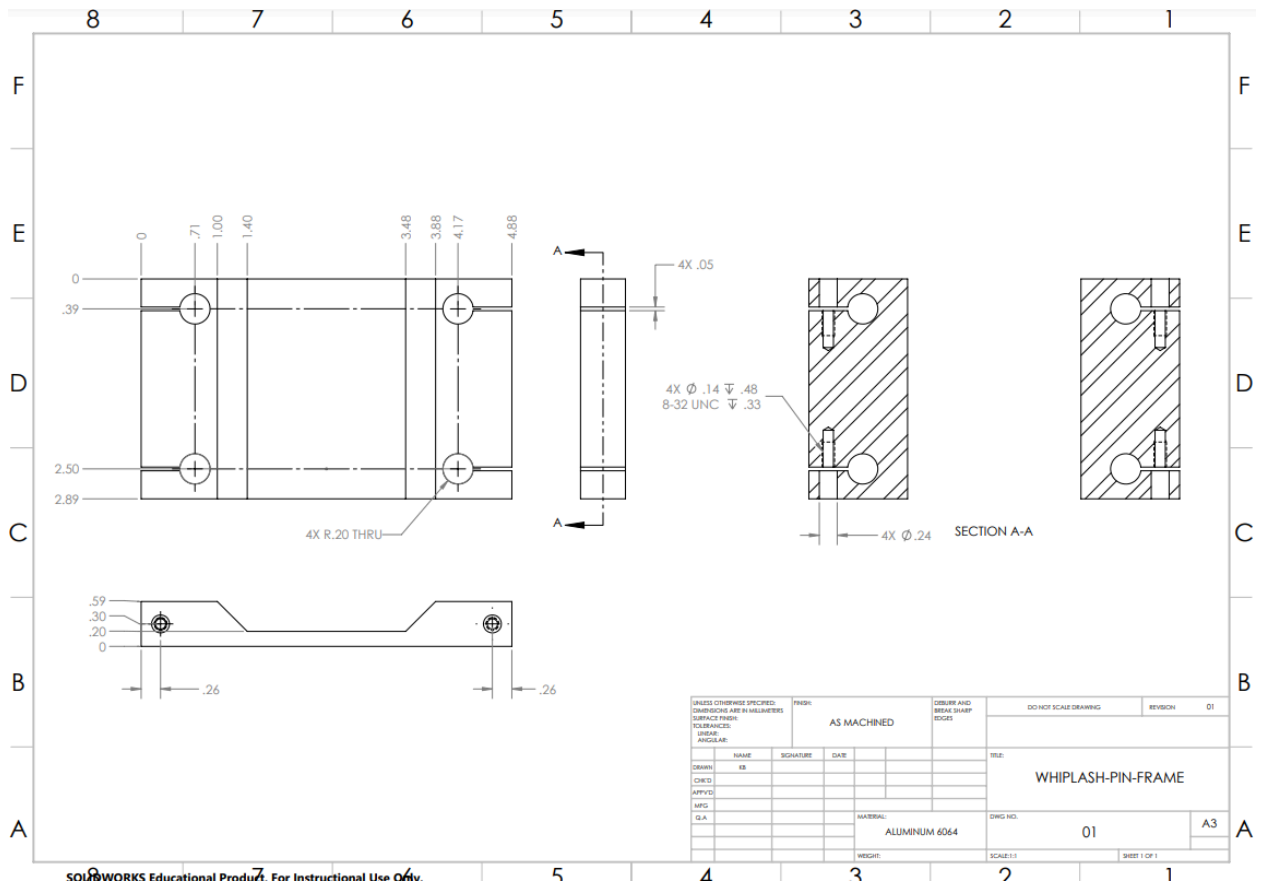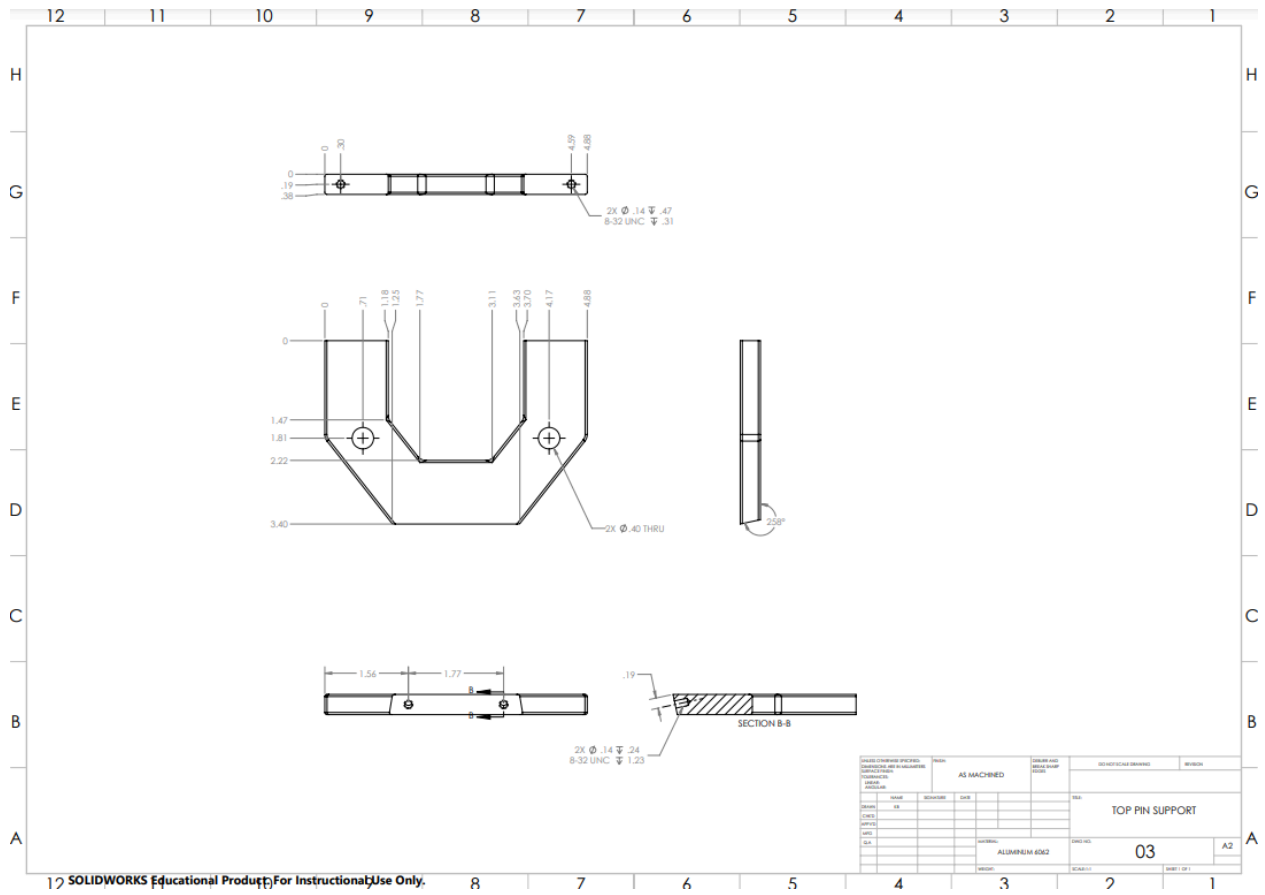

Figure H-4: Back Plate

Figure H-5: Base Mount

Figure H-6: Pin Frame

Figure H-7: Top Pin Support

45